BJS-NA05

Unsteady-State Pressure and Flow Characteristics of the Human Nose: Pre- and Post-Nasal Turbinectomy

A Major Qualifying Project Report:

Submitted to the faculty

of the

WORCESTER POLYTECHNIC INSTITUTE

In partial fulfillment of the requirements for the

Degree of Bachelor of Science

by

Marc R. Guillemette

Waldemar C. Hartung

Mary A. Brock

James S. McLean

January 10, 2007

1. Nose
2. Airflow
3. Turbinectomy
4. Unsteady-State

Prof. Brian J. Savilonis, Advisor

Table of Contents

AUTHORSHIP PAGE ..... **II**

ACKNOWLEDGEMENTS ..... **III**

ABSTRACT ..... **IV**

TABLE OF FIGURES ..... **V**

TABLE OF TABLES ..... **VI**

CHAPTER 1: INTRODUCTION **7**

CHAPTER 2: BACKGROUND **9**

2.1 NASAL ANATOMY 9
2.2 BREATHING CYCLE 12
2.3 BASIC FLUID DYNAMICS 14
2.4 EXPERIMENTAL AND NUMERICAL METHODS 16
2.5 SUMMARY 26

CHAPTER 3: PROJECT APPROACH **27**

3.1 HYPOTHESIS 27
3.2 ASSUMPTIONS 28
3.3 SPECIFIC AIMS 28

CHAPTER 4: DESIGN **28**

4.1 DESIGN CONCEPTS 29
4.2 WATER-TO-AIR DYNAMIC SCALING 29
4.3 SYSTEM DESIGN 33
4.4 COMPONENT DESIGN 34
4.5 VISUALIZATION 39
4.6 LABVIEW EXPERIMENTATION DESIGN 40

CHAPTER 5: METHODS **44**

5.1 VISUALIZATION 44

CHAPTER 6: RESULTS **47**

6.1 PRESSURE AND FLOW DATA 47
6.2 STATISTICAL METHODS 52
6.3 VISUALIZATION IMAGERY 53

CHAPTER 7: ANALYSIS AND DISCUSSION **57**

7.1 PRESSURE AND FLOW 57
7.2 VISUALIZATION 58
7.3 SUMMARY OF FINDINGS 59

CHAPTER 8: CONCLUSIONS **61**

CHAPTER 9: RECOMMENDATIONS **62**

REFERENCES **64**

APPENDIX A: DVD **A-1**

Authorship Page

The team would like to acknowledge each member and present each member's contribution to this report by chapter.

Chapter 1 – Marc Guillemette

Chapter 2 – Marc Guillemette, Waldemar Hartung

Chapter 3 – Waldemar Hartung

Chapter 4 – Waldemar Hartung, James McLean

Chapter 5 – Waldemar Hartung, Marc Guillemette, Mary Brock

Chapter 6 – Marc Guillemette, Mary Brock

Chapter 7 – Waldemar Hartung, Marc Guillemette

Chapter 8 – Marc Guillemette, Waldemar Hartung

Chapter 9 – Waldemar Hartung, Mary Brock

Editorial Review – Marc Guillemette, Waldemar Hartung, James McLean

Acknowledgements

The team would like to extend their sincerest appreciation to the following individuals for their contributions.

Professor Brian J. Savilonis – Professor of Mechanical Engineering at WPI

Dr. David B. Wexler, M.D. – Otolaryngologist at Fallon Clinic

Professor Cosme Furlong-Vazquez – Assistant Professor of Mechanical Engineering at WPI

Michael O'Donnell – Machinist, Manufacturing Department at WPI

Barbara Furhman – Administrative Assistant, Mechanical Engineering Department at WPI

Abstract

A partial nasal turbinectomy is a surgical procedure that opens up the nasal passages to improve breathing. This research obtained quantitative data for the pressure drop across the nasal cavity during unsteady-state flow. In addition, a quantitative and visual analysis of the transition between laminar and turbulent flow was conducted. This experiment implemented a cam-follower system to control the dynamic flow of water through 2X scale acrylic models of an adult nasal cavity, pre- and post-turbinectomy. An experimental pressure versus flow rate curve demonstrates that a linear-laminar region exists followed by a non-linear quadratic region. Furthermore the surgery decreased the total pressure drop. A hysteresis was also observed which is concurrent with clinical observations. These findings suggest that the assumption of quasi-steady flow is invalid. The unsteady-state flow measurements suggest that turbulence is minimized because there is insufficient time for turbulence to develop.

Table of Figures

FIGURE 2.1 ISOMETRIC AND FRONT VIEW OF THE NASAL TURBINATES [1] 10
FIGURE 2.2 DIVISION OF THREE TURBINATE REGIONS WITHIN NASAL CAVITY [1] 11
FIGURE 2.3 TIDAL VOLUME VERSUS TIME, VOLUMETRIC FLOW RATE, AND PRESSURE CHARTS [6] 13
FIGURE 2.4 AIRFLOW AND RESISTANCE COMPARED PRE-FESS VS. POST-FESS [4] 18
FIGURE 2.5 EXPERIMENTAL FLOW CONFIGURATION THROUGH NASAL CAVITY MODEL [9] 20
FIGURE 2.6 RESULTS OF THE RESIN MODEL REPRESENTING NORMAL NASAL ANATOMY [10] 21
FIGURE 2.7 EXPERIMENTAL FLOW CONFIGURATION THROUGH NASAL CAVITY MODEL [12] 23
FIGURE 2.8 EXPERIMENTAL FLOW CONFIGURATION THROUGH NASAL CAVITY MODEL WITH DPIV [3] 24
FIGURE 2.9 PRESSURE VERSUS FLOW CURVE FOR PHYSIOLOGICAL NASAL CAVITY [13] 26
FIGURE 4.1 DISPLACEMENT AND VELOCITY VERSUS TIME PLOTS FROM DYNACAM 35
FIGURE 4.2 CAM PROFILE WITH FOLLOWER AND ROLLER 36
FIGURE 4.3 MANUFACTURED ALUMINUM CAM ATTACHED TO AXEL 36
FIGURE 4.4 SLIDER AND TRACK MECHANISM WITH PISTON AND ROLLER 37
FIGURE 4.5 PISTON HEAD WITH RUBBER O-RING GASKET WITHIN PLASTIC CYLINDER 38
FIGURE 4.6 CLEAR PLASTIC TANK FOR SUBMERSION OF MODELS 38
FIGURE 4.7 COMPLETE ASSEMBLY OF SYSTEM 39
FIGURE 4.8 VISUALIZATION SET-UP 40
FIGURE 4.9 LABVIEW FRONT PANEL OF EXPERIMENTAL VIRTUAL INSTRUMENT 42
FIGURE 4.10 LABVIEW BLOCK DIAGRAM OF EXPERIMENTAL VIRTUAL INSTRUMENT 43
FIGURE 6.1 INHALATION: PRESSURE VERSUS FLOW, PRE-NASAL TURBINECTOMY 48
FIGURE 6.2 INHALATION: PRESSURE VERSUS FLOW, POST-NASAL TURBINECTOMY 49
FIGURE 6.3 EXHALATION: PRESSURE VERSUS FLOW, PRE-NASAL TURBINECTOMY 50
FIGURE 6.4EXHALATION: PRESSURE VERSUS FLOW, POST-NASAL TURBINECTOMY 51
FIGURE 6.5 SIDE VIEW OF THE PRE-OPERATION MODEL, INDICATING TURBINATES, SURGICAL LOCATION AND FLOW DIRECTION. 53
FIGURE 6.6 DYE VISUALIZATION IN THE PRE-OP NASAL MODEL. THE PICTURES ARE NUMBERED TO SHOW PROGRESSION OVER TIME OF THE DYE IN THE NASAL CAVITY. 54
FIGURE 6.7 DYE VISUALIZATION IN THE POST-OP NASAL MODEL 55
FIGURE 6.8 DYE VISUALIZATION IN PRE-OP NASAL MODEL DURING EXPIRATION. 56

Table of Tables

TABLE 2.1: NORMAL BREATHING RATES [6] 14
TABLE 2.2 PRESSURE DROP IN THE HUMAN NASAL CAVITY [7] 17
TABLE 6.1 EXPERIMENTAL TRIAL COMPARISON 52

Chapter 1: Introduction

Enhancing the well-being of human kind has been the life's work of many individuals throughout the course of history. Over the past century the medical field has made profound progress in regards to understanding the human body and developing instruments to detect and treat various maladies. While medicine has been considered more of a general science in the past, it has become a field consisting of many specialized experts. These specialists have divided the human body into hundreds of sections and devoted their lives to try to fully understand each section in its entirety.

In order to improve a patient's breathing it is common in the medical profession to recommend that the individual undergo surgery to help open up the airways in the nasal region. This procedure often involves removing bone and soft tissue in the turbinate region of the nose. Currently, nasal surgery relies heavily upon professional judgment and experience rather than scientific evidence. Very little quantitative evidence regarding the effects of a nasal turbinectomy exists in medical literature. Understanding the pressure-flow characteristics, determining if and where flow separation occurs, and characterizing the flow as laminar or turbulent are essential to developing an understanding of how to perform the ideal turbinectomy; a procedure where the right amount of bone and soft tissue is removed from specific locations to optimize breathing.

To date there has been a significant amount of medical research that has taken steps to achieve a quantitative understanding of the nasal passages. A previous study, conducted by a team of students at Worcester Polytechnic Institute [13], performed experiments on models of a human nose before and after a turbinectomy with the emphasis on measuring pressure drop and flow rate. Measurements were taken at various steady-state flow rates in the pre- and post-operation models. Other research has also been performed which utilizes technologically advanced computational fluid dynamics (CFD) software.

The validity of CFD is questionable because of various limitations of the software: detailed geometry, grid size dependence, and turbulence modeling are only some of the limitations. As a result, much of the CFD research does not provide the scientific and medical community with extensive quantitative data; in addition, other studies that have

developed experimental data have analyzed the human nose only using steady-state flow-rates. This gap between computational and experimental data needs to be addressed in order to have a complete understanding of how surgical procedures affect human nasal passages.

The aim of this project is to address the gap by measuring the experimental data required to understand dynamic flow (i.e. breathing). By designing and constructing an apparatus that will simulate breathing, the team will be able to obtain experimental pressure and flow data that can then be used to develop a better understanding of the effects of nasal surgery on the human nose. There are three explicit goals that will be the key focus of this project;

- Model and measure pressure drop versus dynamic flow
- Determine the transition point of laminar to turbulent flow
- Observe flow separation in pre- and post-operation models

The data that is collected will help verify computational fluid dynamic calculations and influence the future of an ideal nasal turbinectomy procedure; acoustic rhinometry is first used to generate the interior dimensions of the nasal passages, which are then used in a CFD program, where the doctor can perform virtual surgery and test the flow through the nose to develop a customized ideal surgical plan for the patient.

Chapter 2: Background

In order to fully appreciate the scope of the problem that this research addresses, it is necessary to understand several aspects that are pertinent to further research. In the subsequent sections of this chapter the following main topics will be explored:

- The anatomy of the human nose
- The normal breathing cycle
- Basic fluid dynamics; laminar versus turbulent flow
- Experimental methods
- Numerical methods
- A previous study conducted by WPI students

Within each of the main topics there will be a discussion of how this research is relevant to the experiment being conducted. The research has been presented in chronological order to show the progression of the research that has been conducted relating to pressure and flow characteristics of the human nasal cavities. Understanding the human nose and related studies will be valuable in designing, testing, and analyzing a dynamic model of the nasal cavities; therefore, what emerges from this background research is a better understanding of the successes and failures of previous research and where further exploration will be beneficial.

2.1 Nasal anatomy

The human nose, by definition, is the part of the face or facial region in humans that contains the nostrils and the organs of smell and functions as a passageway for air in respiration. The nose is composed of vertebrae that protrude from the center of the human face. The focus of this research is in the nasal cavity that resides behind the nose that is primarily used during at-rest respiration. The nasal cavity is also important because it also serves as part of the respiratory tract that warms and filters air as it is inhaled, as well as containing the organs responsible for the sense of smell. This section will describe the parts of the anatomy of the nose that are essential to this study.

To understand the airflow through the nasal cavity, it is important to understand that there is variability in the surfaces of the cavity. The nasal cavity begins from the anterior tip of the nose and ends at the posterior (where the nasal cavity and throat meet).

The nasal cavities have a very complex geometry which is divided by bone and soft tissue. Figure 2.1 depicts an isometric view of the human nose and a view, which divides the human nose vertically through the center of the nasal cavity.

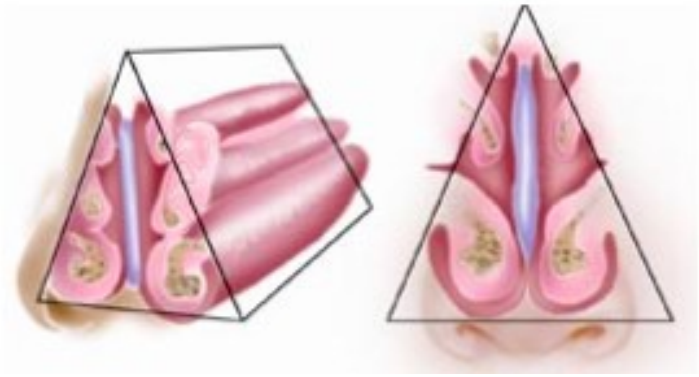

Figure 2.1 Isometric and front view of the nasal turbinates [1]

The anterior region of the nose begins at the tip of the nose or the nasal vestibule. The flow of air begins at this region and the cavity is divided by the cartilaginous septum into two sections. These two sections are recognized as one's nostrils.

It is recognized that the nasal valve region of the nasal cavity is an area that causes a high percentage of airflow restrictions. There are four nasal valves or flow limiting segments: the external valve, the septal valve, the internal valve, and the inferior turbinates [2]. The nasal cavity's cross-sectional area gradually decreases upon connecting with the nasal valve. The nasal valve (internal valve) leads to the next section of the nose that has a much different cross-section than that of the rest of the nasal cavity. In this section of the nasal cavity, the main nasal airway, there are three sections of horizontal outgrowths called turbinates or conchae on each side of the cavity. The three sections of turbinates are (from bottom to top) the inferior, middle, and superior turbinates, as shown in Figure 2.2.

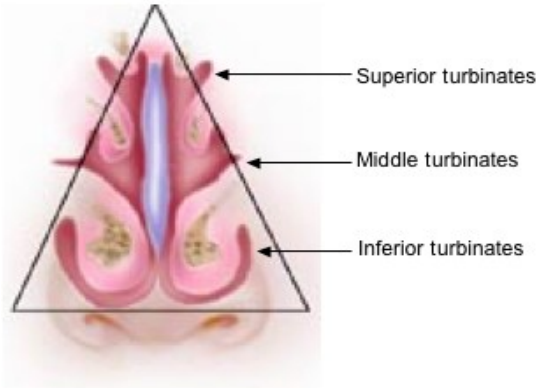

Figure 2.2 Division of three turbinate regions within nasal cavity [1]

The varying cross-sectional areas of the turbinates are a contributor to the complexity of the airflow through the nasal cavity. In the adult nasal cavity, the average height of the nasal roof from the nasal floor in the region of the turbinates is about 40 mm, the width extends about 1-3 mm, and the depth is approximately 60 mm [8].

After the turbinates the two passages of the nasal cavity reconvene into a single passageway. This convening occurs at the end of the inferior turbinate, which leads into the final region of the nasal cavity, the nasopharynx. The airflow in the nasopharynx is directed towards the pharynx, which is then considered part of the throat. The cross-sectional area of the nasal cavity in the region of the nasopharynx increases from the turbinates and is generally not considered the cause of airflow restrictions because the cross-sectional area transition gradually increases.

The turbinates are responsible for redirecting air into specific nasal passages (like the superior turbinate, which contains the olfactory nerve) and for circulating air to moisturize and heat it [3]. Patients who have trouble breathing through their nose are sometimes referred to otolaryngolic surgeons to have a partial or total turbinectomy, which is defined as a partial or total removal of one or more of the turbinates [1].

Unfortunately, many patients can have recurring nasal complications, even after surgery, because it can be difficult for surgeons to gauge how much nasal tissue to excise to minimize breathing obstructions. Until recently, not much research has been done on the fluid mechanics involved. To solve this problem, some scientists have tried to create computerized models of the nasal cavity and to model flow fields [3], while others have taken a more physical approach and used models of actual nasal passages (or collected data from patients) and then measured the flow fields or pressure differences between the turbinates [4, 5].

Even though the research on the effects of the various turbinates and turbinectomies is fairly recent, it has been established that the area above the superior turbinate (where the olfactory nerve lies) “is often vestigial in average human nasal passage” and that only about 14% of inspired air reaches that area [3]. One study found that the excision of the middle turbinate caused little to no problems in patients, and patients who have had it removed were found to have a significant decrease in nasal

resistance, thus making it easier for them to breathe [4]. The inferior turbinate appears to have the most effect on airflow, which makes sense since it is the first structure that inhaled air comes in contact with and thus provides most of the swirling effect. There has been very little and often times conflicting research that explains the flow characteristics during expiration, but Cook et al. found that the air received "virtually no resistance" [4]. Oppositely, Keyhani et al. concluded that "though velocity profiles were smaller the turbinate still causes some resistance" [8]. The conflicting research suggests that further analysis of expiration is needed to address this gap in understanding the full dynamic breathing cycle.

2.2 Breathing cycle

In 1964, Fenn et al. published their work [6] which provided a quantitative analysis of the tidal volume versus time in a normal adult breathing cycle through the nasal cavity. The derivative of tidal volume with respect to time, volumetric flow rate, and pressure changes are of great importance because any research must follow these relationships in order to successfully mimic breathing. Figure 2.3 depicts these relationships for an adult nose as concluded by Fenn et al.

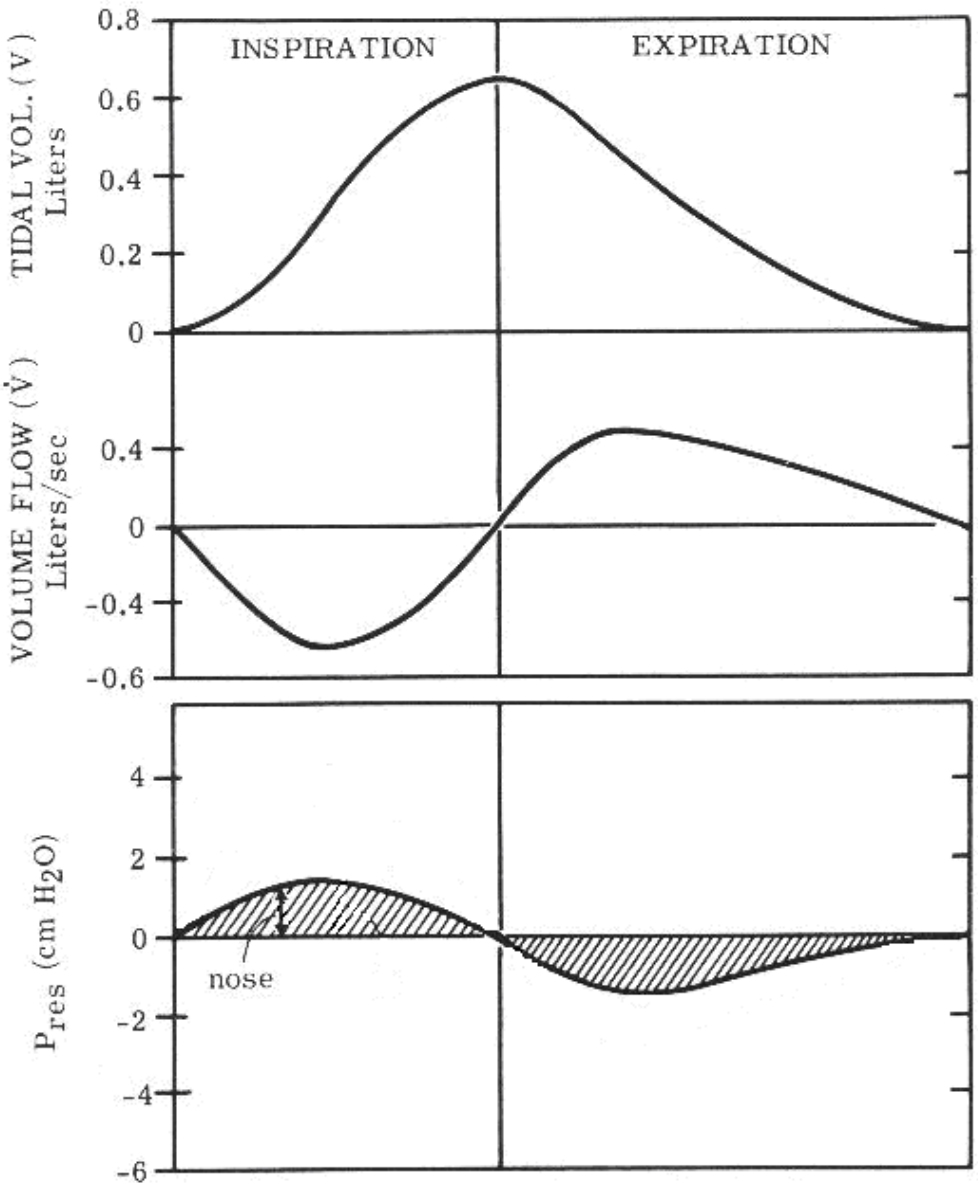

Figure 2.3 Tidal volume versus time, volumetric flow rate, and pressure charts [6]

As deduced from Figure 2.3, the maximum pressure during inhalation is approximately 1.7 cm of H_2O and the maximum total pressure during exhalation is approximately 1.5 H_2O, which supports the idea that there is slightly less resistance to flow during exhalation.

It is also important to have a general understanding of the range of breathing parameters. In every individual there is some variability in a breathing cycle.

Table 2.1 shows the typical breathing rates in breaths per minute (bpm) for normal breathing.

Table 2.1: Normal breathing rates [6]

Typical breathing rates		
	Low (bpm)	High
Adult	12	20
Teenager	16	25
Preschool	20	30
Infants	20	40
Newborns	44	

Normal breathing changes from nose to mouth once the individual requires more oxygen than can be provided from the nose alone. This is a result of heavier breathing rates usually caused by exercise or physical activity.

The understanding of where the airflow is distributed throughout the nasal cavity will be very important in order to analyze and draw conclusions from further research. In addition a detailed analysis of the physiology of the human nose allows one to make educated hypotheses in regards to the way the human nasal cavities might respond to experimental conditions (i.e. changes in flow rates, etc.).

2.3 Basic fluid dynamics

The primary objective of this research is to identify flow separation and whether the flow separation can be characterized as laminar or turbulent. What is flow separation? When an object is subjected to fluid flow moving at some velocity, the no-slip condition is assumed and a boundary layer develops over the surface of the object. The particles in contact with the surface of the object have are static. As one moves further out from the surface of the object, the particles continuously acquire some velocity. Once the edge of the boundary layer is breached the particles will have the free stream velocity or the initial velocity of the fluid. The boundary layer is a result of friction between the fluid's molecules and the object's rough surface. Flow separation will occur when the boundary layer experiences a very large adverse pressure gradient. An adverse pressure gradient is when the fluid particle experiences a very large, positive,

$$\frac{\partial p}{\partial x} \qquad \textbf{Eq. 2.1}$$

This causes the fluid particle to decelerate and detach from the surface. This results in the fluid field forming an eddy or vortex. What is important to establish is that flow

separation does not imply or require turbulence. One can have laminar flow and still have controlled flow separation. Whereas, when one has chaotic flow separation, turbulent flow can be assumed. Studies have shown that once flow separation is obtained, the relation between pressure and flow is nonlinear.

Laminar flow can be characterized as fluid particles in smooth layers, or lamina. Turbulent flow is one in which the fluid particles randomly and rapidly mix due to the three dimensional velocity fluctuations with respect to time. Turbulent flow is undesirable since it results in a higher resistance to flow; however it also provides rapid mixing which enhances heat and mass transfer. When characterizing whether the flow is laminar or turbulent, one must estimate the Reynolds number.

$$\mathrm{Re} = \frac{4Q}{\pi D \nu} \qquad \textbf{Eq. 2.2}$$

Here, Q is the volumetric flow rate, D is the characteristic diameter, and ν is the kinematic viscosity. The Reynolds number is the ratio of inertial forces to vicious forces. The Reynolds number must be weighed against the critical Reynolds number to determine whether the flow is laminar or turbulent. This depends on the flow configuration and must be determined experimentally. For flow in a pipe the critical Reynolds number is usually assumed to be 2,300. Thus, when looking at fully developed flow in a pipe, flows with a Reynolds number below 2,100 would be considered laminar. For flows with a Reynolds number above 3,000, the flow is generally dominated by inertial forces producing random eddies, vortices, and velocity fluctuations. Therefore, critical Reynolds number identifies the point of transition between laminar and turbulent flow.

When modeling breathing one must consider the effects of unsteady flow and how the critical Reynolds number is affected as a result of unsteady flow. Studies have shown that the critical Reynolds number can be related to the Womersley number

$$We = R\sqrt{\omega/\nu} \qquad \textbf{Eq. 2.3}$$

R is the appropriate length scale, ω is the frequency, and ν is the kinematic viscosity. The Womersley number is the ratio of pulsatile flow frequency to vicious effects. Studies have shown that Womersley numbers approaching unity are said to be near the critical value. This is the point where the inertial forces and vicious forces are in balance. The

low frequency ranges, termed pre-critical, have dominant vicious effects, while the high frequency ranges, termed post-critical, have predominantly inertial effects. In the pre-critical range, viscous forces become rapidly dominated by impulse forces (changes in pressure gradient), resulting in a sharp drop of the critical Reynolds numbers with increasing Womersley numbers. In the post-critical range, inertial forces become increasingly dominant over impulse forces, resulting in flow stabilization. In the limits, as Womersley approaches zero or infinity the critical Reynolds number approaches a constant value. In other words pulsating flow destabilizes the fluid flow.

2.4 Experimental and numerical methods

To fully develop a plan for further experimental research, it is necessary to acquire an understanding of previous studies that have been conducted in the field of otolaryngology. Though there have been many experimental, computational and theoretical explorations in this field, the following research presented in this section will clearly explain what conclusions have already been established and which areas still require more investigation.

In 1993, a study was conducted by Hahn et al. that used a 20X scale model of the human nose. This study was primarily focused on studying the nasal airflow patterns of the human nose. The study collected velocity profiles of several sections of the human nose using a hot-film anemometer. The 20X scale model that was used was created using computer axial tomography scans, conventionally known as CAT scans, to generate an anatomically accurate model of a healthy adult's right nasal cavity. The extravagant size of the model allowed for the detailed regions of the nasal cavity to be easily investigated without disrupting flow patterns with experimental equipment. A wide range of steady flow rates (180, 560, and 1,100 mL/s) were produced to mimic normal and heavy adult inspiratory and expiratory breathing rates through the right side of the human nasal cavity.

This research supported the notion that airflows in the nasal cavities can be turbulent, but is arguably laminar throughout most of the nasal cavity. As Hahn et al. stated, "airflows were determined to be moderately turbulent, but changes in the velocity profiles between the highest and lowest flow rates suggest that for normal breathing laminar flow may be present in much of the nasal cavity" [7]. These findings can be

directly related to this research as the team determines if and when turbulent flow exists in the pre- and post-operation models. It is expected that the post-operation model would incur less turbulence than that of the pre-operation model because resistance is supposed to have decreased as a result of the surgery.

Pressure characteristics of the large-scale model were also measured in this experiment. The pressure drop across the nasal cavity was estimated from the average total shear stress measured at the central nasal wall. It was stated thusly, "the overall longitudinal pressure drop inside the nasal cavity showed good agreement with literature values measured in human subjects" [7]. This notion directly supports the hypothesis that pressure characteristics of the human nasal cavity can be mimicked experimentally and therefore can be used to support computational fluid dynamic modeling. Table 2.2 contains the experimental data that was collected compared to the calculated expected values. The data was scaled to a 1X scale from the 20X scale model.

Table 2.2 Pressure drop in the human nasal cavity [7]

Pressure drop in the human nasal cavity		
Flow Rate (mL/s)	Calculated ΔP (cmH_2O)	Measured ΔP (cmH_2O)
1,100	4.5	6.0-17
560	2.3	1.5-4.3
180	0.4	0.26-0.74

Another study [4] of a partial middle turbinectomy focused on understanding changes in nasal airflow and resistance after the surgical procedure. This study is recognized as the first study to look at the effect of middle turbinectomies (total or partial). The goal of this 1995 study was to collect quantitative data from 31 patients who were undergoing functional endoscopic sinus surgery (FESS). The range of ages included ages 8 to 70 years old and a ratio of 1.38 males to females [4]. An anterior rhinometer was used to measure airflow and pressure drop across the human nasal passages and data was collected from both the left and the right nostril for comparison.

This research is significant because of a notable decrease in pressure difference across the nose that was observed after the surgical procedure. In addition, an increase in airflow was also observed after the surgery. Figure 2.4 depicts the results that were obtained by the study.

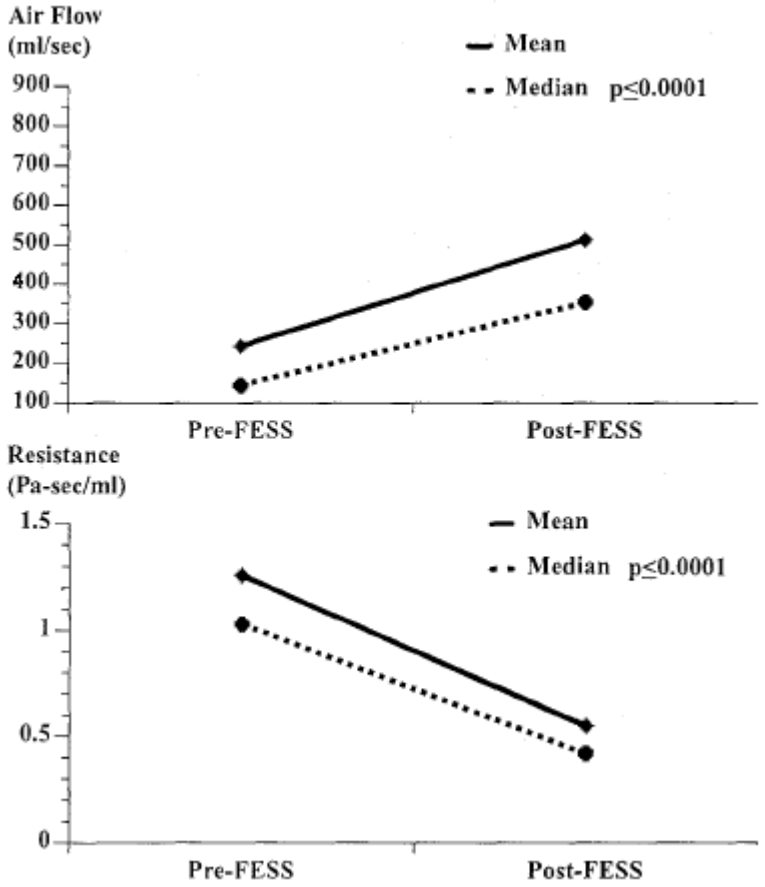

Figure 2.4 Airflow and resistance compared pre-FESS vs. post-FESS [4]

The mean ± standard deviation of nasal airflow (at 150 Pa) before surgery and after surgery was reported at 243 mL/s ±213 mL/s and 510 mL/s ±427 mL/s, respectively. The median of the airflow data before and after surgery was reported at 145 mL/s and 354 mL/s, respectively. Resistance was statistically reduced for post-op patients. Cook et al. also noted that the noticeable changes in airflow and resistance did not adversely affect patients' comfort. In another important statement by Cook et al., it was concluded that,

> "...because of the middle turbinates' modest surface area, decreased density of erectile and vascular tissue, less prominent position in the patterns of nasal airflow, and anatomic differences compared with that of other mammals, the middle turbinate was of less functional significance than the inferior turbinate" [4].

This study provides significant evidence that turbinectomies do indeed improve airflow within the human nasal cavity by reducing resistance up to 50% and increasing airflow in the nasal cavity by almost 300%.

Another important aspect of the study of pressure and flow characteristics of the human nasal passages is the introduction of numerical simulations. In 1995, Keyhani et al. [8] looked to develop quantitative methods to describe and measure airflow patterns of the human nasal cavities. The objective of their research was to develop numerical methods so that objective methods to assess nasal surgery would become available.

As part of the study, an anatomically correct finite element mesh of the right human nasal cavity was constructed from CAT scans of a healthy adult nose. The finite element mesh was then analyzed by numerically solving two governing equations: the steady-state Navier-Strokes equation, which models laminar flow, and the mass conservation equation for incompressible steady flow. Also assumed in these calculations was that "the walls of the nasal cavity were assumed to be rigid, and at the interface between air and the surface of the cavity the no-slip boundary condition was applied" [8]. The Strouhal number, a dimensionless parameter of the ratio of unsteady acceleration and convective accelerations, was determined to be much less than one and was used to decide that the quasi-steady approximation could be considered valid. These equations were used to determine laminar airflow patterns in the nasal cavity at low breathing rates (approximately 125-200 mL/s with Reynolds number equal to 610 at the nostrils).

Inspiratory and expiratory flows were mimicked experimentally, studied and then compared to the numerical calculations from the finite element mesh. As Keyhani et al. stated, "…the numerical results agreed with experimental measurements in the physical model to within 20 percent at most comparison locations" [8]. When compared to the results obtained by Hahn et al. there were discrepancies, which were attributed to both numerical and experimental errors. The source of experimental error was accounted for by natural convection effects that can occur in low velocity measurements and the uncertainty associated with the location of the hot-film anemometer. Discrepancies in the effort to match the finite element mesh with the same geometry as the physical model, as well as the grid dependency of the meshing, attributed for the source of numerical error.

The study yielded several conclusions, which helped to describe airflow characteristics of the human nasal cavity. It was found that nearly 30% of the inspired volumetric flow passed below the inferior turbinate. During expiration, it was found that these velocities were noticeably smaller. When compared to the numerical simulation, the

experimentally measured velocity field results provided validation that during at-rest breathing, airflow is laminar [8].

Kelly et al. [9] conducted another study in 2000 that explored laminar and turbulent type flows. Particle Image Velocimetry (PIV) was used to determine the two-dimensional instantaneous velocities. PIV is an optical method used to measure instantaneous velocities in fluids. This study, like many other studies, isolated one nostril so that flows could be analyzed easier without interference with the other side of the nasal cavity. A model was constructed from 26 computed tomography scans of a healthy right adult nasal cavity. Using a pump and valve configuration as shown in Figure 2.5, water was used as a medium for flow rates in the nasal cavity model. Both inhalation and exhalation were separately modeled and tested in this experiment, but this research still only considered steady-state flows.

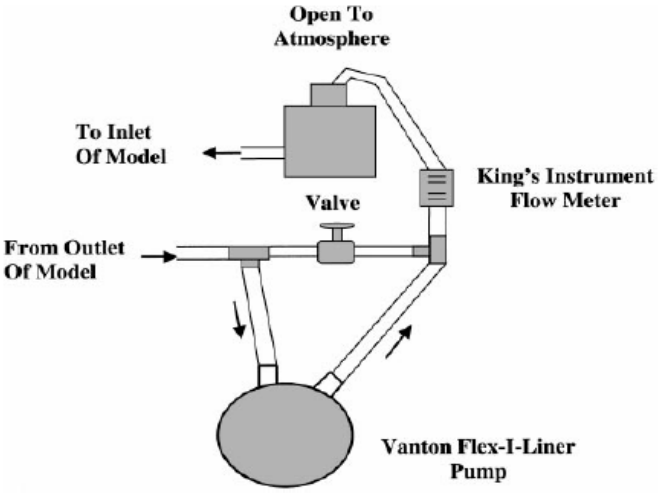

Figure 2.5 Experimental flow configuration through nasal cavity model [9]

The study focused on obtaining an experimental validation of the location of laminar and/or turbulent type flows throughout the nasal cavity as a result of various steady non-oscillatory flow rates. A major component of this validation was flow visualization using dye, which was injected outside the nostril into the model. As observed by Kelly, "a major proportion of flow passed through the middle airway…and a small fraction of the flow separated upward, forming a standing eddy in the olfactory area" [9]. It was concluded that these findings suggested that some turbulence exists in the nasal cavity. Flow rates of 100 mL/s to 300 mL/s were tested in the 2X scale model. It was found that at 125 mL/s predominantly laminar flow was observed and only at 208 mL/s was

turbulent flow observed [9].

In 2003, Ivo Weinhold and Gunter Mlynski [10] published their work which furthered the research in numerical simulation of airflow in the human nose. Weinhold and Mlynski developed and validated a method for the numerical simulation of the airflow through the human nose. In their research two anatomically correct resin models were used in conjunction with CAT scans of two patients. One resin model and one clinical model represented an unaltered human nasal cavity and the other models represented a nose after pathological alterations. Utilizing FloWorks 2001, a computational fluid dynamics package, the velocity and pressure fields in these models were calculated for a range of volumetric flow rates between 20 mL/s and 1,400 mL/s [10] through one side of the nasal cavity.

Figure 2.6 depicts a combination of the results obtained experimentally from the resin model that represented the normal nasal cavity, its estimated tolerance, and the corresponding numerical simulation.

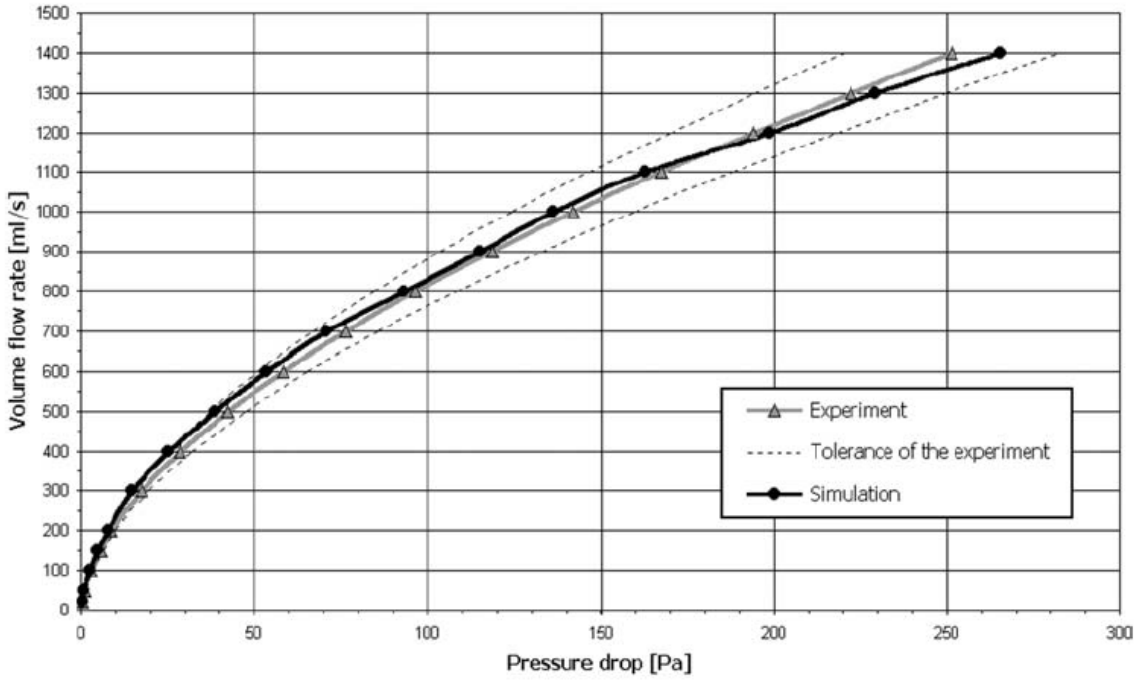

Figure 2.6 Results of the resin model representing normal nasal anatomy [10]

It was concluded that the results from the computational fluid dynamics package were within the tolerance of the experimental data. Weinhold and Mlynski stated that, "the quantitative evaluation of the simulated flow pattern in the nasal cavity of the patient with normal anatomy confirmed the understanding of a normally ventilated nose" [10].

Weinhold and Mlynski also concluded that the development of numerical models of the human nasal cavity is still a very time consuming and error-prone process. It was determined that numerical simulations are still not cost effective enough to become a commonly used tool for otolaryngologists [10], The technology is soon approaching a cost effective equilibrium, but there are enough technical considerations that need to be addressed to make geometrical reconstruction automated; which would inherently make it a more powerful and effective tool. The results obtained from this experiment support that in the near future, computational fluid dynamics software can be a substitute for experimental research. The current study of unsteady-state pressure and flow characteristics of the human nose will be an extension of this research and will also fill gaps in previous research; including effects of inhalation and exhalation, and the effectiveness of a partial nasal turbinectomy.

In 2004, Neil A. Bailie presented some further research in the field of computational fluid dynamics (CFD) methods in conjunction with understanding modeling fluid flow through the human nose. The objective of this research was to develop accurate numerical models using CFD. Bailie states that, “it is the intention that accurate models of the fluid flow within the nasal passages will assist rhinoplasty (nasal surgery)” [11]. CAD models were generated from nasal CAT scans of healthy volunteers using specialized computer software and then the CAD models were used to accurately generate meshes (3 dimensional grids) of the nasal cavities [11]. Using numerical predictions from the software package, a comparison was made between these predictions and the experimental data obtained from the solid model. Bailie concluded, “the results of the numerical simulations showed agreement with the experimental results and with the results of the previous experimental studies within the literature [11]. Part of the analysis tried to develop some understanding of the variations between different individuals. These variations were noticeable yet not completely explainable. It is the hope of Bailie that “numerical simulation of nasal airflow using computational fluid dynamics techniques will offer a novel, noninvasive method of assessing of nasal airflow and related phenomena. Alteration of the computer model can be performed to simulate pre-operatively the results of nasal surgery (virtual surgery), which may be of considerable clinical benefit” [11]. Further research resides in continuing the validation of CFD

techniques as well as developing an understanding of how surgeries will affect different patients.

Churchill et al. [12] conducted another 2004 study which addressed the morphological variation and airflow dynamics of the human nasal cavity. This research continued to explore the characteristics of nasal flow regimes (i.e. laminar, transient, and turbulent). In order to test these characteristics water was used to mimic physiological flow rates (adjusted for dynamic similarity). Dyes were also used and injected into the flow in anatomically accurate acrylic models of the human nasal passages. In this study the models were derived from direct casting of 10 cadavers. Figure 2.7 demonstrates the nasal airflow experimental set-up that was used for this research.

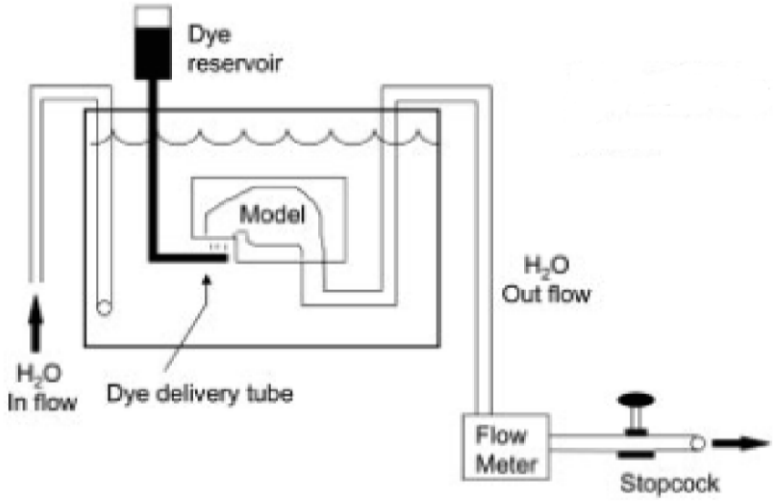

Figure 2.7 Experimental flow configuration through nasal cavity model [12]

The experiment plotted results from steady-state flows and led to the conclusion that "the projecting turbinates appear to laminate flow rather than induce turbulence" [12]. Importantly, it was noted that within the experiment there was considerable variation in both the flow regimes and the principle pathways. This study addressed inhalation solely and did not provide an understanding of pressure differences in the models.

In a study conducted in 2006, Hörschler et al. investigated how the geometry of the nose affects flow during inspiration and expiration. They assumed that intricate details of the nose, like mucous and hairs, did not affect flow enough to be included in their calculations. They also assumed that the effects of the superior turbinate were negligible because "it is often vestigial in average human nasal passages" [3]. Their

experimental model had two main components on the surface of the nasal passages: cartilage spurs (located at the septum) and the turbinates.

There were five physical and numerical models used: (1) one with no spurs and no turbinates, (2) lower turbinates only, (3) upper turbinates only, (4) upper and lower turbinates only, and (5) spurs and both turbinates. The authors flushed the water/glycerol mix through their transparent nose models, which were contained in a tank, and aerated the solution with small hydrogen bubbles in order to measure the flow with a camera and Digital-Particle Image Velocimetry (DPIV). The design schematic for this experiment is shown in Figure 2.8.

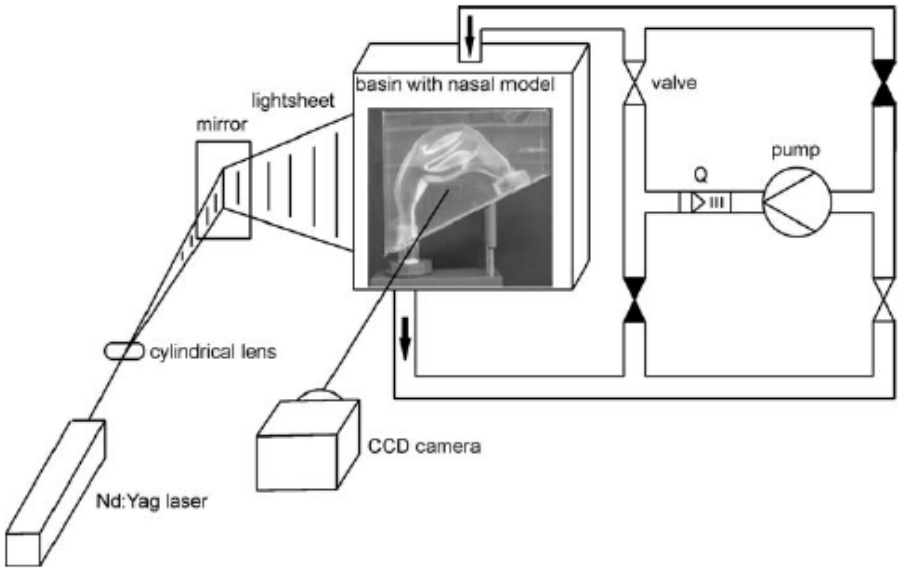

Figure 2.8 Experimental flow configuration through nasal cavity model with DPIV [3]

For inspiration, the authors approximated a flow of 159 ml/s, and expiration was 127 ml/s (with Re of 500 and 400, respectively). The Reynolds numbers were calculated based on approximate throat diameter. Importantly, the flow was found to be laminar at these numbers. Inspiration velocity was estimated at 0.4 m/s, and expiration was 0.2 m/s. Later, the authors used higher Reynolds numbers (790 and 1,000), but found no statistical difference between the results for the change in Reynolds number. The pressure gradients were measured non-dimensionally and pressure drops were observed to be independent of varying Reynolds numbers.

When the experiment was completed, the authors compared velocity fields in cross sections of both numerical and physical models and found a very strong correlation.

When the numerical and experimental data was compared, it was concluded that the interior geometry of the nose, with spurs and turbinates, was optimized for inspiration so that when one breathes in, air is mixed and swirled sufficiently (since one of the main functions of the turbinates is to humidify and affect the temperature of the incoming air, and swirling increases the amount of air that touches the inner surface of the nasal cavity) [3]. The inferior turbinate was the one that was found to have the most impact on flow, since it was the first turbinate that air was likely to come in contact with. During expiration, the geometry of the nose was found to not have a significant effect on flow, which was attributed to the increase in cross-sectional area in the nasal cavity and a lower resistance.

A previous research project, conducted by students at Worcester Polytechnic Institute in 2005 [13], began to explore the effect that changes in physiological flow rates has on human breathing. This study utilized 2X life-size models of the human nasal passageway: one pre-turbinectomy and one post-turbinectomy. The objective of the research was to experimentally explain the effectiveness of a partial nasal turbinectomy.

In order to create an effective experimental set-up, water was used to replicate physiological breathing through the models. The study utilized a differential pressure transducer to measure the pressure drop across each of the models from the entrance at the nostrils to the entrance to the throat or nasopharynx. Water flow rates were controlled to correspond to several simulated physiological breathing rates. Each of these flow rates was tested individually on each of the models to develop an understanding of the effects of the partial nasal turbinectomy. The results were then plotted to graphically represent a pressure-flow relationship. These curves were then used to determine if and when the flow characteristics in the nose change from laminar to turbulent flow. In addition, a visual study was conducted using dye injection to observe the transition of flow characteristics from laminar to turbulent.

It was shown that the data could then be divided into two sections: one range of flow-rates less than 300 cc/s and one range of flow rates greater than 300 cc/s. The flow rates less than 300 cc/s were determined to be best fit with a linear regression, whereas the larger flow rates followed a quadratic regression. Figure 2.9 depicts the pressure-flow curve that was developed from the experimental data.

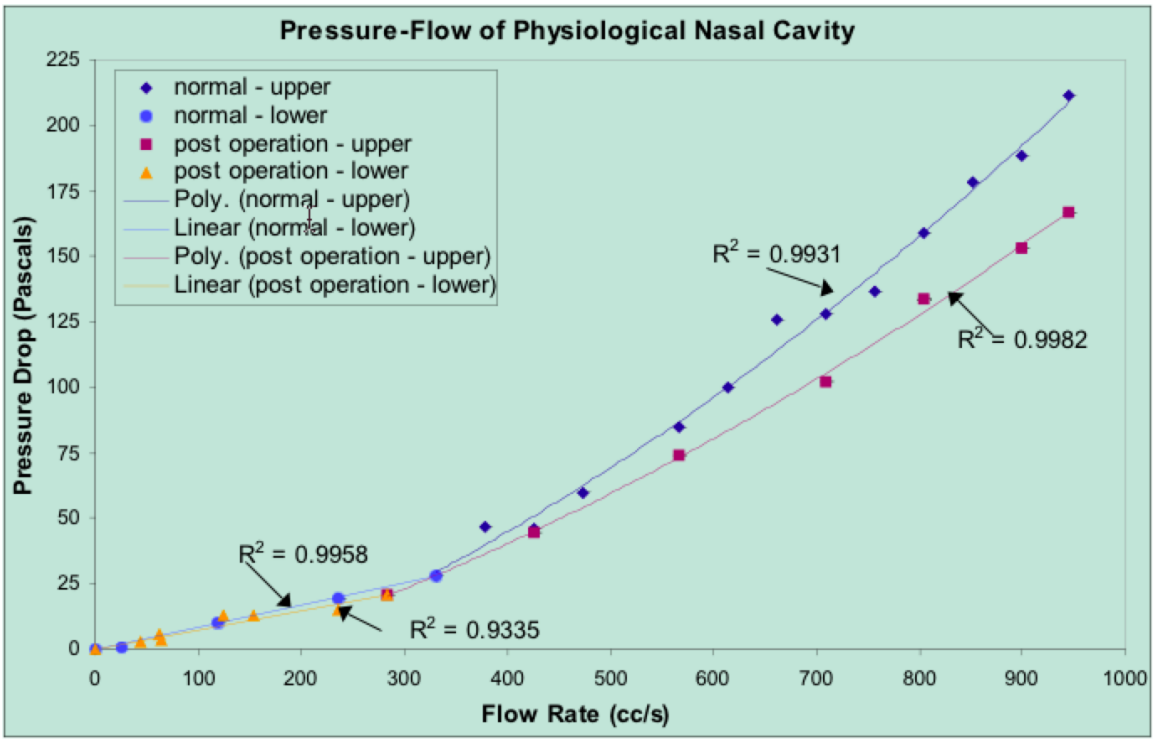

Figure 2.9 Pressure versus flow curve for physiological nasal cavity [13]

It was deduced that the quadratic relationship suggested turbulent resistance in the nasal passages. The experimental data was also complimented with visualizations that provided some evidence to support these conclusions.

This study provided a significant amount of experimental data but a lack of understanding of what might occur during dynamic flow rates still exists. The next step in understanding the effects of a partial nasal turbinectomy is to collect pressure data from a model that simulates unsteady-state breathing.

2.5 Summary

The information presented in this chapter is a general overview of the necessary information required to have an understanding of the experiment that will be presented in the subsequent chapters. The key points that were outlined in this chapter include: the basic physiological anatomy of the human nose, the normal breathing cycle, basic fluid dynamics, and the experimental and numerical models that have previously been used to analyze the pressure and flow characteristics of the human nose.

Chapter 3: Project Approach

In this chapter the strategy for this study will be outlined: specifically, the hypotheses that will be tested and implemented, the assumptions that will constrain and focus the work, and the specific aims that will justify this approach.

3.1 Hypothesis

Based on an analysis of prior research, the aim of this project is to simulate unsteady flow in the nasal passages and generate a pressure versus flow rate curve. Once the pressure versus flow rate curve is defined, additional efforts can be focused on determining the point at which the relation between pressure and flow rate deviates from linearity. In previous research this deviation was found to occur in steady flow at approximately 300 cc/s through both nostrils. To establish this, emphasis will be placed on looking at the pressure differential across the nasal passage, and plotting the pressure differential as a function of time. Knowing the theoretical flow rates that are generated during a breathing period, an expression can be formulated that relates the pressure differential as a function of flow rate. Doing this for the pre- and post-turbinectomy models, the changes in the maximum pressure drop and the point at which linearity transitions can be established. It is hypothesized that a turbinectomy will reduce the maximum value of the pressure differential across the nose and increases the value in which non-linear flow separation begins. This would imply that it would take a smaller pressure difference to generate a particular flow rate, resulting in easier breathing.

Apart from the emphasis that is put forth on looking at the onset of flow separation, additional efforts will be put towards analyzing the onset of turbulence and flow separation, since both can be characterized by non-linear behavior. Visualization will be the key to differentiating turbulence versus flow separation. Studies have shown that the critical Reynolds number at which turbulence begins occurs with higher frequencies in steady flow, but since the flow is unsteady, flow separation maybe reduced since vortices may not have enough time to develop.

3.2 Assumptions

It is well known that the viscosity of a fluid is dependent on temperature. During normal breathing air is subjected to temperatures varying from 25 C° to 35 C°. The corresponding viscosities of air at these temperatures are $1.84x10^{-5}$ N*s/m^2 and $1.88x10^{-7}$ N*s/m^2 respectively. For the purpose of this experiment it will be assumed that the temperature of air is constant during breathing, although the air that passes into one's lung is exposed to the higher body temperature. Looking further, it is well known that humans breathe in air and exhale carbon dioxide; it will be assumed that the chemical composition during the course of normal breathing is constant.

It is assumed that the breathing that will be scaled is that of a person who is breathing about 10 breaths per minute and with a tidal volume of 0.5L. This corresponds to an average volumetric flow rate of 5 liters per minute. It was assumed that the density of air is approximately 1.2 kg/m^3 and the viscosity of air is $1.84x10^{-5}$ N*s/m^2.

3.3 Specific aims

The goal is to construct a device that will simulate normal breathing within the nasal passages (i.e. simulate unsteady flow) for the pre- and post-operation models. With a device that simulates the flow field within the nasal passages; volumetric flow will be plotted against pressure drop. Since the pressures that are of key interest fall within the linear portion of the flow versus pressure curve, careful consideration must be taken so that the pressures that are measured have a minimal uncertainty. This requires assuring that there are minimal vibrations, external loads are filtered out, and that the data acquisition system has the appropriate resolution. It is critical that pressure versus time curve is repeatable. With a plot of pressure versus flow rate, an understanding of how a turbinectomy affects normal breathing can be obtained. In the experimental setup visualizations must also be easily attainable so that any flow separation that occurs can be identified as either laminar or turbulent.

Chapter 4: Design

The following chapter is aimed at developing a thorough understanding of the design of the experiment. The subsequent sections will walk through the process that was

used in order to create a breathing simulation device. The selected design follows an iterative process which involved scaling water flow characteristics to air flow characteristics and thus setting the boundary conditions for design. A cam-follow system was implemented which requires the profile on the cam to rotate about a fixed point which displaces the piston through the cylinder forcing water through the nose models. After the explanation of the initial design concepts, the necessary calculations and relationships will be presented first to lay the foundation for the rest of the design, followed by a detailed description of the design, and then the experimentation methods.

4.1 Design concepts

When looking at previous research, there were very limited studies which addressed unsteady flow. Most of the previous experimental research only looked at steady-state flow. Initially it was though that one could use a pump to generate the unsteady flow, but after a feasibility study, cost drove the need for another alternative.

When looking for a pump that could generate the required flow, the real challenge was that the required flow would be continuously changing and reversible. Much of the difficulty with the pump was not only finding a pump that was reversible, but one that was continuously reversible: that is to say, a pump that could reverse flow without having to be shut down and manually reversed. In addition, the cost of the pump was also a concern. As a result of the limited funding, it would not be economic to spend a majority of the funds on a pump.

Since it was critical to have a continuous dynamic flow, it was concluded that this could be achieved through the use of a piston and a cylinder driven by a cam. In addition, the piston and cylinder would prove to be more cost-effective than the pump. The only primary draw back is that each component of the device would have to be designed and built and certain changes would have to be made in the scaling factors.

4.2 Water-to-air dynamic scaling

When determining ways to simulate fluid flow through the nasal passages, there were two dimensionless variables that needed to be scaled, Reynolds Number and Womersley number. The Reynolds number (Re) is defined as the ratio of inertial forces to viscous forces and is represented by the following expression;

$$\mathrm{Re} = \frac{4Q}{\pi D \nu} \qquad \textbf{Eq. 4.1}$$

This number is also often used to describe the onset of turbulence. In fully-developed pipe flow $Re_{critical}$ is equal to 2,300, but it can vary by orders of magnitude depending on the system.

The Womersley number (α) is a parameter used in biomechanics. It is an expression which relates unsteady acceleration to vicious forces and is defined by the following expression;

$$\alpha = \frac{D}{2}\sqrt{\frac{\omega}{\nu}} \qquad \textbf{Eq. 4.2}$$

In the expressions above, D is the characteristic diameter of the nose, ω is the flow frequency, Q is the volumetric flow-rate, and ν is the kinematic viscosity.

These dimensionless numbers are essential to simulating normal breathing flow rates, similar to the actual flow characteristics observed inside the nasal passages. By assuring that these constants were scaled correctly for this system, the simulated flow inside the pre- and post-operation models can be assumed to be related.

Starting with the Reynolds number, since the models supplied were twice the size of a normal nose, this constrained the flow rate and the kinematic viscosity. When deciding what medium (air or water) would be used to simulate the flow, it was decided that flow visualization was critical. In the medical field having visualizations is important when verifying flow separation or turbulent flow. With this in consideration, water was chosen as the medium that would be used to simulate the flow. With the kinematic viscosity of air being 1.5×10^{-5} m^2/s, switching to water reduced ν by a factor of 15.

With the following constraints put on D and ν, the scaled volumetric flow rate can be calculated. Recalling flow similarity, Re* will represent the simulated flow, and Re will represent the actual flow; thus, Re*=Re. Substituting for the scaled values and simplifying:

$$\frac{Q^*}{D^* \nu^*} = \frac{Q}{D\nu} \qquad \textbf{Eq. 4.3}$$

Simplifying,

$$Q^* = Q\frac{D^*}{D}\frac{\nu^*}{\nu}$$
$$Q^* = Q \times \frac{2}{1} \times \frac{1}{15} \qquad \textbf{Eq. 4.4}$$

This asserts that the flow simulated must be 2/15 the scale of the actual flow generated within the nasal passages, or that airflow will be 7.5 times that of the flow of water used in the experiment.

When designing the device, it was important to know what the total volume of fluid that would be drawn in over the course of one cycle was. The total volume was relevant since the design would require a force to displace the quantity of water. The volumetric flow rate would be generated by the displacement of the piston and was related to the cross sectional area of the cylinder by the following equation:

$$Q^* = A\frac{dl}{dt} \qquad \textbf{Eq. 4.5}$$

This expression was useful when determining the displacement profile for the piston head, but what was also pertinent in determining the size of the cylinder. The average Q could be expressed by the following equation:

$$Q_{avg} \approx 2V \times \omega \qquad \textbf{Eq. 4.6}$$

The two is a result that it takes half a period to draw in the total volume V. Utilizing the principles of similar flow,

$$Q^*_{avg} = \frac{2}{15}Q_{avg} \qquad \textbf{Eq. 4.7}$$

Looking at the Womersley number and applying similar flow, it can be concluded that;

$$\omega^* = \frac{\omega}{60} \qquad \textbf{Eq. 4.8}$$

Thus,

$$V^*\omega^* = \frac{2}{15}V \times \omega$$
$$V^* = \frac{2}{15}V \times \frac{\omega}{\omega^*} \qquad \textbf{Eq. 4.9}$$
$$V^* = \frac{2}{15}V \times 60 = 8V$$

What is important to recognize is the independence on the medium when scaling the total volume. The total volume is independent of the medium, and is only dependent on the cube of the scaled diameter. As a result, once the diameter is chosen there is only one exact volume that will satisfy Womersley and Reynolds. The average human breathes in 0.5 liters of air per breath; this requires that the device must include a cylinder with a total volume of 4 L operating at a frequency of 0.17 rpm, assuming a standard breathing cycle of 10 breaths per minute. From these constraints, it was concluded that these parameters had a significant bearing on the size of our cam, the size of the piston head, the amount of friction involved, and the size of the motor. These factors also had an effect on the amount of time that would be required to construct the device. Having a cam with a smaller stroke and a smaller piston head would reduce the amount of friction in the device and the amount of power required needed to operate the system.

Looking at the effects that these conclusions had on the profile of the cam, it was determined that the cam profile was dependent on dl/dt, but the size of the piston head was dependent on the cross sectional area. Combining the above equations yielded the following result:

$$A\frac{dl}{dt} = 2V^{*}\times\omega^{*}$$
$$A\frac{dl}{dt} = 2\times 8V\times\omega^{*} \qquad \textbf{Eq. 4.10}$$

Looking at the above expression, by increasing the area one reduces the profile of the cam, but increases the size of the piston and visa versa. Thus, it was necessary to choose a volume that was smaller than the specified scaled value. Unfortunately, the problem that would arise is that the Reynolds number and Womersley number could not both be satisfied.

To reanalyze this it will be relevant to redefine the Reynolds number in terms of the breathing frequency and the total volume.

$$\frac{V^{*}\omega^{*}}{D^{*}\nu^{*}} = \frac{V\omega}{D\nu}$$
$$\omega^{*} = \frac{V\omega}{V^{*}}\times\frac{\nu^{*}}{\nu}\times\frac{D^{*}}{D} \qquad \textbf{Eq. 4.11}$$

By looking at this expression, if one chooses not to scale the V, V*=V, than one must rescale the breathing frequency. The problem is that referring to the Womersley number, the breathing frequency has already been defined; therefore, the problem lies within finding a breathing frequency that best maintains an appropriate value on the Reynolds number and the Womersley number. Since it was important to have good pressure responses, the Reynolds number took precedence. Thus,

$$\omega^* = 10rpm \times \frac{1}{15} \times \frac{2}{1} \times \frac{V}{V^*} \qquad \textbf{Eq. 4.12}$$

Therefore, choosing a smaller V* increases ω*. What is crucial is that a small change in ω has a significant effect on the Womersley number. As a result, the construction of the piston and cylinder system was constrained by the following boundary conditions;

$$\omega^* \cong 5.5rpm$$
$$V^* \cong \frac{2}{15}V \qquad \textbf{Eq. 4.13}$$

Calculating a Womersley number based on these calculations, it can be determined that the diameter of the channel would be multiplied by a factor on the order of approximately 1,100. This provides sufficient evidence that the critical Reynolds number will not be compensated as a result of the Womersley number since it is far from unity.

4.3 System design

The initial objective, prior to looking at the pre- and post-operation models, was to construct a device that would simulate unsteady flow (breathing) through a 2X nose model. The scaling analysis provided sets of criteria that would have to be satisfied. Ideally in order for both Womersley and Reynolds to be satisfied:

$$\omega^* = .25rpm$$
$$V^* = 4.8l \qquad \textbf{Eq. 4.14}$$

Thus,

$$Q^*_{avg} \cong 2(4.8L).25rpm \cong \frac{2}{15}Q_{avg} \qquad \textbf{Eq. 4.15}$$

The primary principle in generating the appropriate flow rate is expressed in the following equation:

$$Q^* = A\frac{dl}{dt} \qquad \textbf{Eq. 4.16}$$

Since it was evident to reduce the amount of friction, limitations had to be put on the maximum cross sectional area that could be used. In addition the values on the cross sectional area was limited to the available tubing that could be purchased directly, as apposed to directly manufacturing the cylinder.

$$Q^* \cong 2V^*\omega^*$$
$$Q^* \cong 2AL\frac{1}{\tau} \qquad \textbf{Eq. 4.17}$$

Thus by specifying the cross sectional area we have specified the piston stroke; the period was already specified via Womersley by the frequency. It was then difficult to satisfy both the Reynolds number and Womersley number. The trade off is that the Womersley number will be off by 472% as the Reynolds is close to the appropriate scaled value by 34%. (for a detailed analysis refer to the Appendix).

$$\frac{\omega-\omega^*}{\omega}\times 100\% = 472\%$$
$$\frac{\mathrm{Re}-\mathrm{Re}^*}{\mathrm{Re}}\times 100\% = 34\% \qquad \textbf{Eq. 4.18}$$

As a result of the findings in the appendices, the following constraints were concluded:

$$\omega^* = 5.5rpm$$
$$A = 3.8cm$$
$$L = 7cm \qquad \textbf{Eq. 4.19}$$
$$V^* = .08liters$$

4.4 Component design

The following section details the design of each of the components of the cam-follower system. Each component will be presented with a detailed description and explanation of its purpose and function.

Cam design

When constructing the cam the first step involved generating a profile that defined the volume intake versus time. Figure 2.3 from the background research was used to generate a scaled breathing function. By dividing each point on the curve by the specified

area and then multiplying by a factor of 2/15, a curve was generated that represents the displacement of the piston head versus time.

Using DynaCam the displacement profile was used as a reference when constructing the cam profile. Since it was difficult to achieve a smooth profile by specifying every point on the curve, a spline function was used. The spline function allowed different sections of the curve to be shifted, in order to achieve a curve that mimicked the theoretical one, while still preserving a cam with a smooth profile. The DynaCam plots of displacement and velocity versus time are shown in Figure 4.1 and demonstrate that a curve identical to that of the theoretical tidal volumes and volumetric flow rates can be generated.

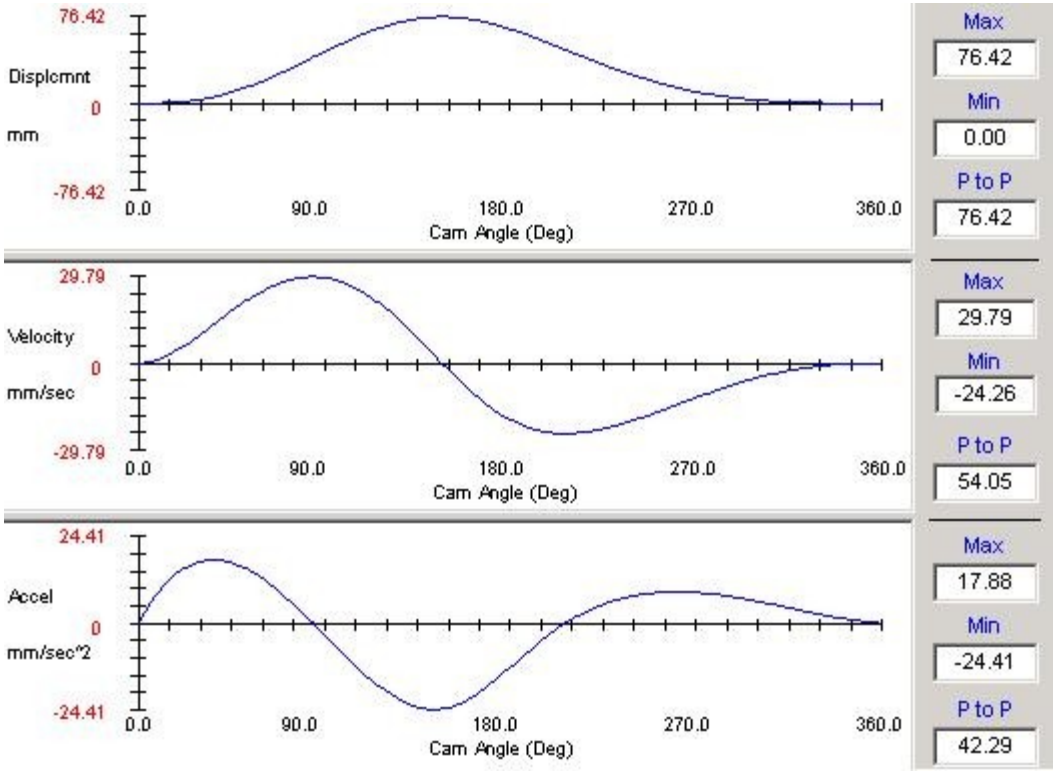

Figure 4.1 Displacement and velocity versus time plots from DynaCam

Figure 4.2 was the next step in designing the cam. This figure is a representation of the cam profile with a follower and roller which must be designed in relation with the cam.

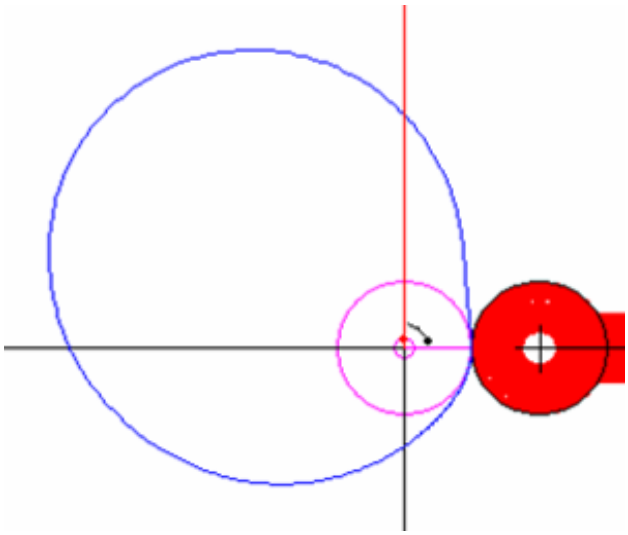

Figure 4.2 Cam profile with follower and roller

When the cam profile was completed, it was mapped to a CAD file to be manufactured. Aluminum, a readily available material, which is light and durable, was used to manufacture the cam. The CAD file was then mapped to GibbsCAM which provides a programming language that can be interpreted by computer numerical control (CNC) milling machines. The thickness of the cam is 1 cm and approximate diameter is 10 cm. The manufactured cam is shown in Figure 4.3.

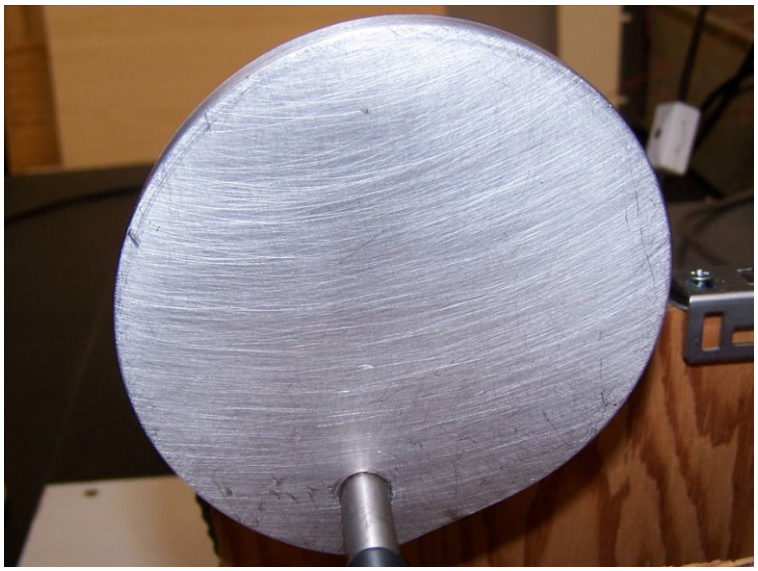

Figure 4.3 Manufactured aluminum cam attached to axel

Slider design

The slider was constructed in order to keep the connecting rod and the piston aligned. This was done in order ensure that the piston slides in and out of the cylinder

without pushing into the sidewalls and creating more friction than necessary. The slider is shown in Figure 4.4.

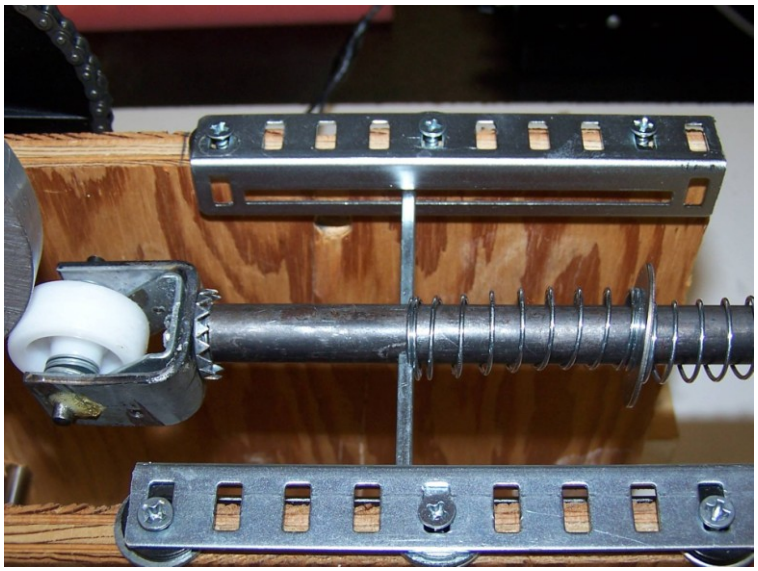

Figure 4.4 Slider and track mechanism with piston and roller

Piston

The piston head was made slightly less than the diameter of the cylinder by 2 mm. It was ideal to have a less than tight fit, to reduce friction. The seal between the cylinder wall and the piston head was achieved with a gasket. The friction resulting from the gasket and cylinder wall was reduced using generic silicone grease. There was a 1 mm groove cut around the top of the piston head to allow for the gasket. It was quickly determined that using a lubricant that was water soluble was unsuccessful; thus silicone was used as a lubricant. The piston and cylinder are shown in Figure 4.5.

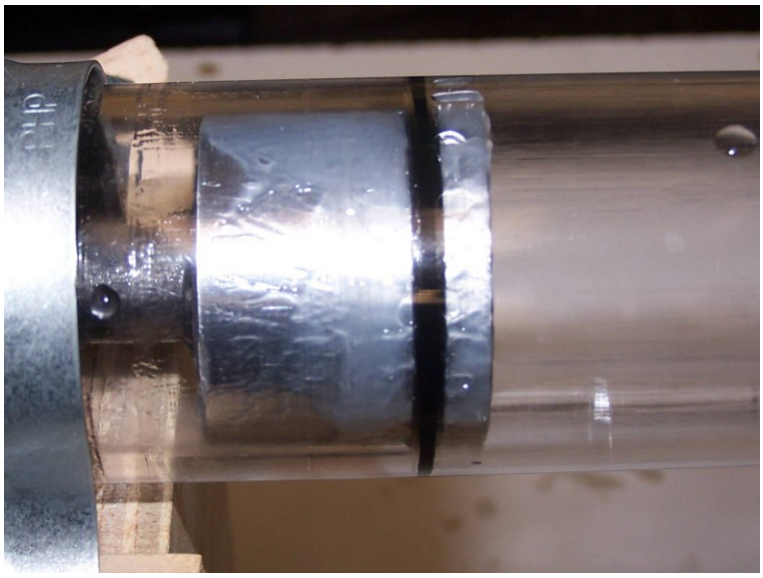

Figure 4.5 Piston head with rubber o-ring gasket within plastic cylinder

Tank

The tank was designed with a clear plastic, Lexan, so as not to compromise visualization. The size of the tank was designed, keeping in mind two basic needs: it had to fit the model, and had to be big enough to allow for modifications and placement of data acquisition and visualization equipment. The tank is shown in Figure 4.6.

Figure 4.6 Clear plastic tank for submersion of models

Assembly

The entire assembly, including each of the system components, is shown in Figure 4.7. As can be seen in the figure, the piston-cylinder part of the assembly was connected to the tank via plumbing piping, PVC piping, and tube clamps.

Figure 4.7 Complete assembly of system

4.5 Visualization

When designing the setup for visualization, the basic concept was to inject a dye into the flow field and record how the dyed particles responded to the flow field. The biggest problem was that the dye response depended on the point in the cross-sectional area the dye was injected; careful methods had to be utilized that controlled the stability of the dye intake. A coat hanger was deformed and taped to the side of the tank, so that the tip of the injection tube sits at the tip of the nasal entrance. Thin plastic tubing was then taped parallel to the coat hanger and the end from which dye exited was centered in the cross-section at the tip of the nose. For a diagram of the visualization setup refer to Figure 4.8.

Figure 4.8 Visualization set-up

4.6 LabVIEW experimentation design

When constructing the experimental setup, careful consideration was given to the placement of the data acquisition system and the resolution of the device. The pressures that were expected to be measured were approximately from 0.7 Pa to 215 Pa. The main concern was the lower pressures, since it was expected that the lower pressures would be critical in defining the initial linear potion of the pressure versus flow curve. As a result of the lower pressure constraint, one of the nostrils of the nose models would be plugged. This decision forces flow through one nostril which will allow a larger pressure measurement to be taken at the entrance to the nose and this decision also isolates the right turbinate where the surgery was performed.

The estimated resolution of the data acquisition was calculated to be

$$\frac{range}{2^{number\_of\_bits}} \qquad \textbf{Eq. 4.20}$$

The range was concluded to be a +10 V to -10 V ranges, and the data-acquisition was found to consist of 16 bits. Thus

$$resolution = \frac{20}{2^{16}}$$
$$resolution = 0.3mV \qquad \textbf{Eq. 4.21}$$

This implies that the data acquisition could recognize changes no smaller than 0.3mV.

The pressure transducer that was used during this experiment was a PX138-.305V (for a list of the specifications refer to the Appendix). The pressure transducer was found to generate a 1 V to 6 V output ±0.3 V, based on an 8 V excitation. This equates to

$$S = \frac{5V}{4137Pa}$$
$$S = 0.0012\frac{V}{Pa} \qquad \textbf{Eq. 4.22}$$

The expected measured pressures were to be no lower than 0.5 Pa. This small value corresponds to an output voltage of 0.6 mV; thus due to the uncertainty of the device the actual voltage could be 0.2 mV or 0.9 mV. More efforts could have gone into amplifying the signal, but since pressure versus flow at very tiny flow rates is linear, this region was not of much concern. Therefore, it was concluded for the regions of concern, the resolution available would suffice.

Following the external hardware setup, the LabVIEW virtual instrument (VI) was constructed. The main objectives of the VI were to read voltages and then implement a transfer function to map it to a corresponding pressure. One of the main calculations in the VI was to divide the output signal voltage from the pressure transducer by the source voltage or excitation voltage. This would allow the results to be independent of the excitation. The VI was defined to sample anywhere from 15 to 30 data points per minute and then writes them to a spreadsheet. Figure 4.9 and Figure 4.10 are the user interface panel and the internal programming structure, respectively (for an extensive look at the VI refer to the Appendix).

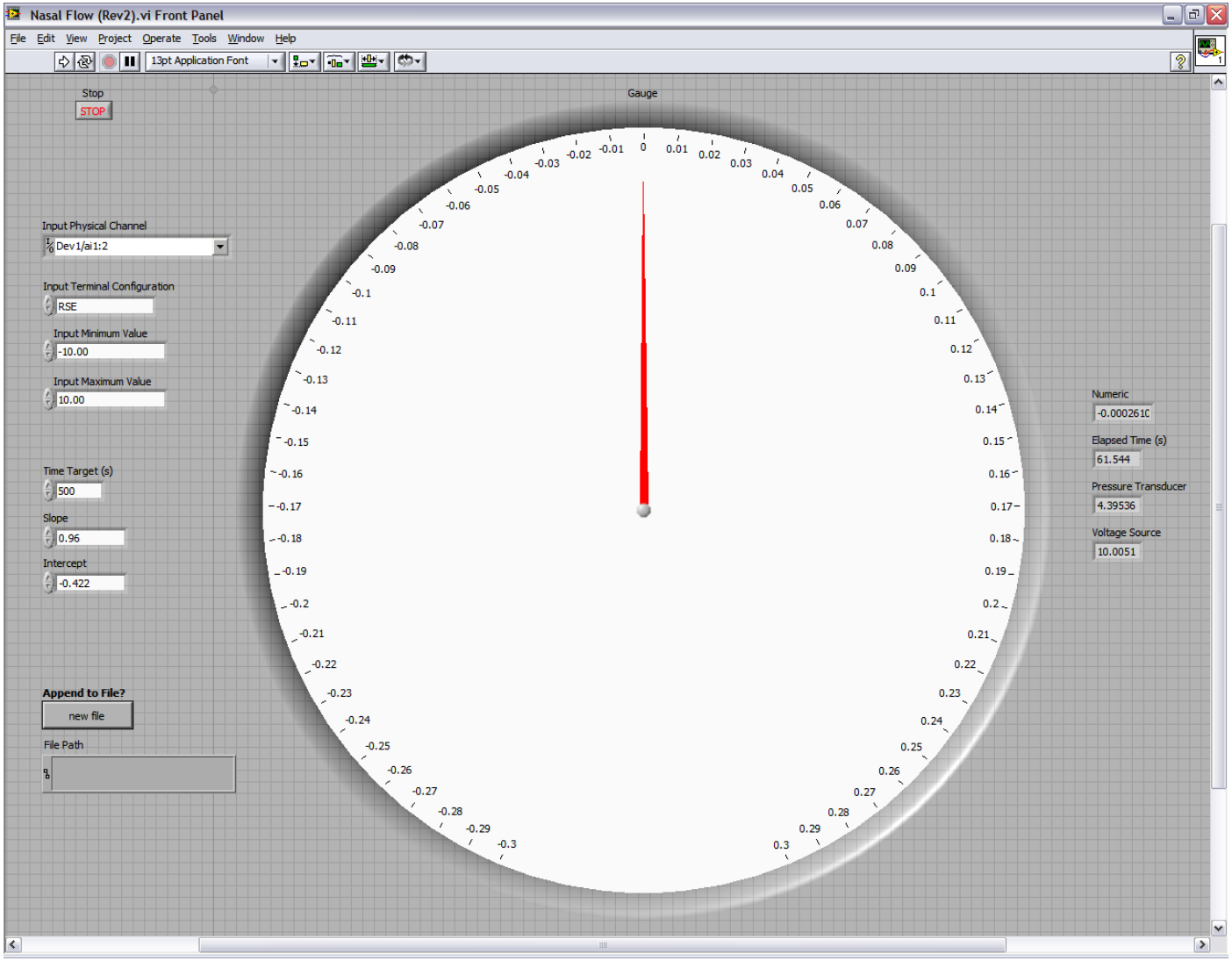

Figure 4.9 LabVIEW front panel of experimental virtual instrument

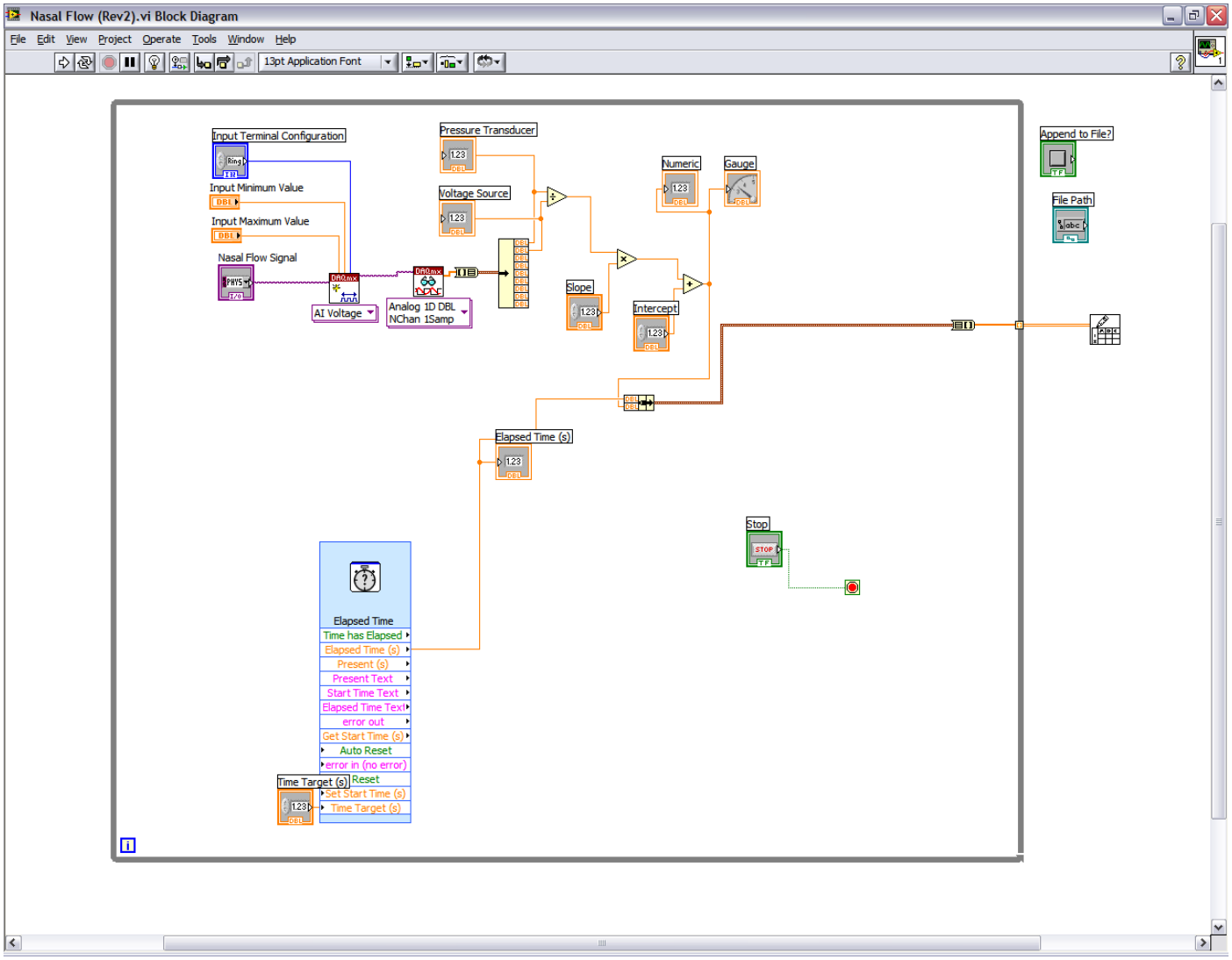

Figure 4.10 LabVIEW block diagram of experimental virtual instrument

Chapter 5: Methods

In this section the methodology of this experiment will be described in detail. There are two crucial elements to this study:

- Pressure drop measurements
- Visualization observations

Each of these elements is crucial to verify the hypotheses, specifically that the onset of flow separation is characterized by a non-linear relation when pressure is plotted versus flow rate. The pressure drop measurements will help to better understand when the onset of flow separation occurs. Turbulence may be determined if chaotic vortices are observed through visualization. These will lead to a comprehensive understanding of how flow behaves in the human nasal cavity, specifically identifying the point at which flow separation occurs and characterizing the flow separation as being laminar or turbulent.

5.1 Visualization

Due to the fact that flow visualization is important to assure credibility of the results, efforts were put forth to optimize visualization clarity. Efforts consisted of improving the methods that were used in the previous MQP setup. The improvements consisted of lining the back of the tank with white paper, to create a greater contrast when recording the dye. A high quality digital camcorder was used to record the flow in the models. The recording was analyzed and stills from the video were taken to display the flow field at different times during a single pulse. In was pertinent to show not only flow separation during inhalation, but also the difference in flow between inspiration and exhalation. After the stills were taken, the pictures were enhanced and clarified using Adobe Photoshop.

To produce the actual visuals, it was decided to use regular water-soluble food coloring to produce the visual of air swirling around in the nose without damaging the nose model. The design setup consisted of filling a syringe with dye, hooking it to a small tube, and securing the last half of the tube to a coat hanger. This was found to better stabilize and position the end of the tube. During the inhalation phase, the syringe was slowly pushed down, since it was pertinent to only release a small amount of dye so that

diffusion and flow would be easier to discern. The dye was injected with the direction of the flow within the nasal cavity. This was necessary so as to not add momentum to the fluid. LabView and pressure data acquisition

When taking the pressure measurements, the nose was submerged completely in water. The differential pressure transducer was connected to the two ends of the nose via tubing. The setup is shown in Figure 4.8.

What must be recognized is, for the given setup, what are the actual pressures that are being measured? Look at the unsteady Bernoulli expression.

$$P_1 + \rho\frac{1}{2}V_1^2 + \rho z_1 g = P_2 + \rho\frac{1}{2}V_2^2 + \rho z_2 g + h + \rho\int_1^2 \frac{dV}{dt}ds \qquad \textbf{Eq. 5.1}$$

In this expression h is the head loss due to friction. The equations for inhalation and exhalation are shown in Equation 5.2 and Equation 5.3, respectively.

$$P_1 - (P_2 + \rho\frac{1}{2}V_2^2) = h + \rho\int_1^2 \frac{dV}{dt}ds - \rho\frac{1}{2}V_1^2 + \rho g(z_2 - z_1) \qquad \textbf{Eq. 5.2}$$

$$(P_1 + \rho\frac{1}{2}V_1^2) - (P_2) = h + \rho\frac{1}{2}V_2^2 + \rho\int_1^2 \frac{dV}{dt}ds + \rho g(z_2 - z_1) \qquad \textbf{Eq. 5.3}$$

Prior to any measurements the pressures were taken when the flow was not pulsating, zero velocity, thus,

$$P_1 - P_2 = \rho g(z_2 - z_1) \qquad \textbf{Eq. 5.4}$$

Since the height differential is the same throughout any cycle the pressure transducer was zeroed by adding a constant, thus for inhalation what was being measured was:

$$P_1 - (P_2 + \rho\frac{1}{2}V_2^2) - \rho g(z_2 - z_1) = h + \rho\int_1^2 \frac{dV}{dt}ds - \rho\frac{1}{2}V_1^2 \qquad \textbf{Eq. 5.5}$$

And for exhalation,

$$(P_1 + \rho\frac{1}{2}V_1^2) - (P_2) - \rho g(z_2 - z_1) = h + \rho\frac{1}{2}V_2^2 + \rho\int_1^2 \frac{dV}{dt}ds \qquad \textbf{Eq. 5.6}$$

Thus for inhalation, if it was found that the maximum value for the pressure differential was α where $\alpha > 0$ then

$$h - \rho V_1^2 + \int_1^2 \frac{dV}{dt} ds = \alpha$$

$$h = \alpha + \rho V_1^2 - \int_1^2 \frac{dV}{dt} ds \qquad \textbf{Eq. 5.7}$$

Thus the head loss could be less than that of what is actually measured, due to the unsteady term. The unsteady term could be positive or negative depending on what point is being observed during the inhalation.

For exhaling, if it is found that the maximum value for the pressure differential was –β where β > 0 then

$$h' + \rho V_2^2 + \int_1^2 \frac{dV}{dt} ds = -\beta$$

$$h' = -\beta - \rho V_2^2 - \int_1^2 \frac{dV}{dt} ds \qquad \textbf{Eq. 5.8}$$

$$|h'| = (\beta + \rho V_2^2 + \int_1^2 \frac{dV}{dt} ds)$$

Thus the head loss h' during exhalation could be greater or less then what is actually measured. Analysis was done on approximating the acceleration term during peak flow rates.

$$\rho \int_1^2 \frac{dV}{dt} ds \approx \left(\frac{dV}{dt} \right)_{avg} S \qquad \textbf{Eq. 5.9}$$

Here S is the length of the streamline, which can be approximated by the distance between the inlet and outlet.

$$\left(\frac{dV}{dt} \right)_{avg} \qquad \textbf{Eq. 5.10}$$

Equation 5.10 is a value that averages the acceleration, when integrating along the streamline.

What is crucial is that the head loss is not equal to the head loss prime. This is due to the fact that the head loss is dependent on the flow field and the orientation of the probe. The VI read pressure measurements form the pressure transducer, 30 readings per minute, and recorded the values to a excel file, where they were analyzed and interpreted.

Chapter 6: Results

The completion of the experiment yielded two important findings. The findings are detailed and presented in the following chapters which are divided into two separate parts; experimental data for pressure versus flow and visualization observations.

6.1 Pressure and flow data

It is important to recognize that during the data acquisition process, pressure measurements were taken and recorded versus time. From the DynaCam plots (refer back to Figure 4.1), the flow rates were then mapped to specific time instances within a cycle. Thus, the pressure measurements can then be directly correlated to volumetric flow rates. It is also important to note that these values apply to one nostril only.

After performing the necessary scaling, the pressure data that was collected for the model with water running through the nasal cavity model were converted back to a 1X scale nose breathing air. The results were then split into inhalation and exhalation for comparison purposes. Figure 6.1 depicts the scaled results for inhalation within the pre-operation nose model.

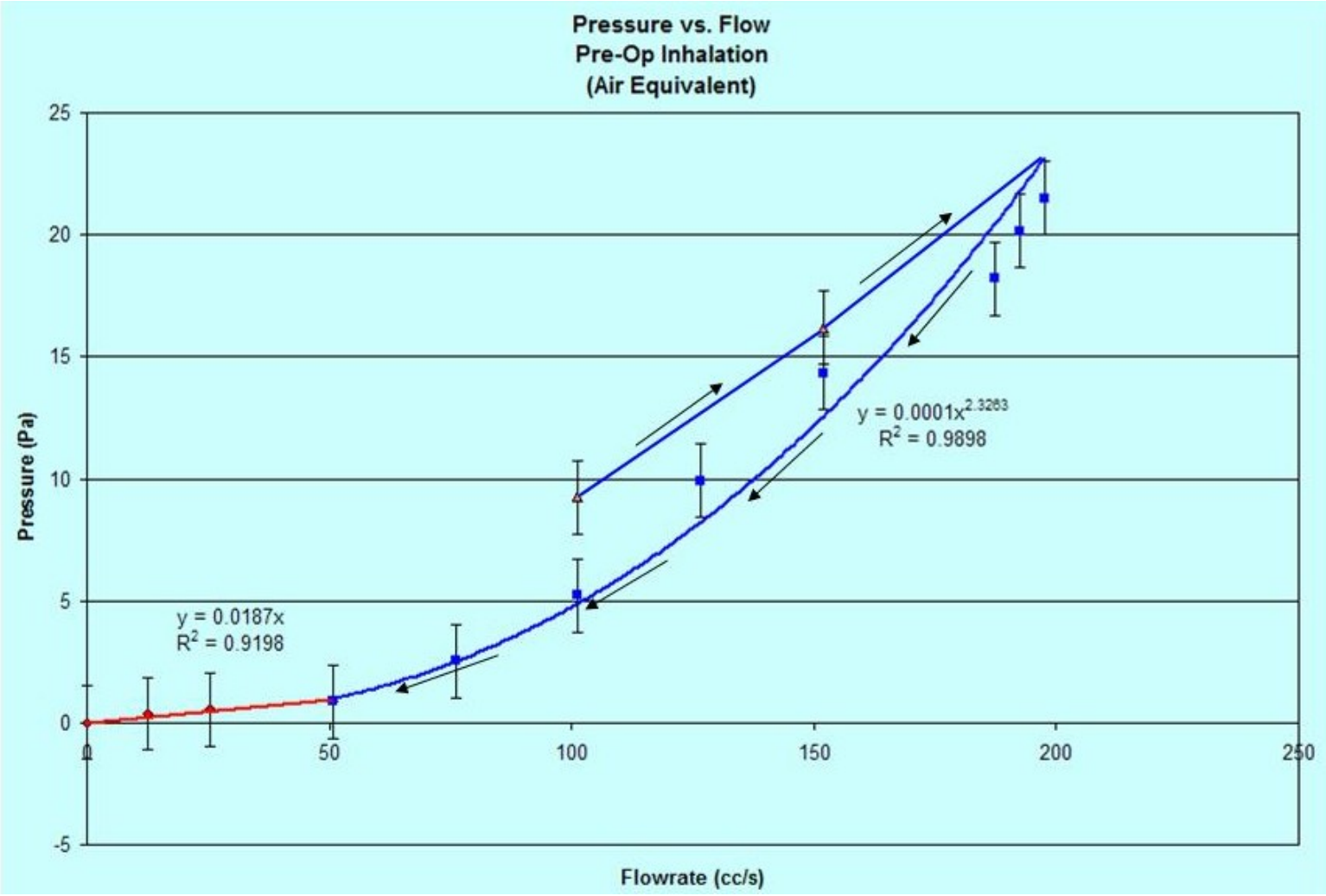

Figure 6.1 Inhalation: pressure versus flow, pre-nasal turbinectomy

Figure 6.2 depicts the scaled results for inhalation within the post-operation nose model.

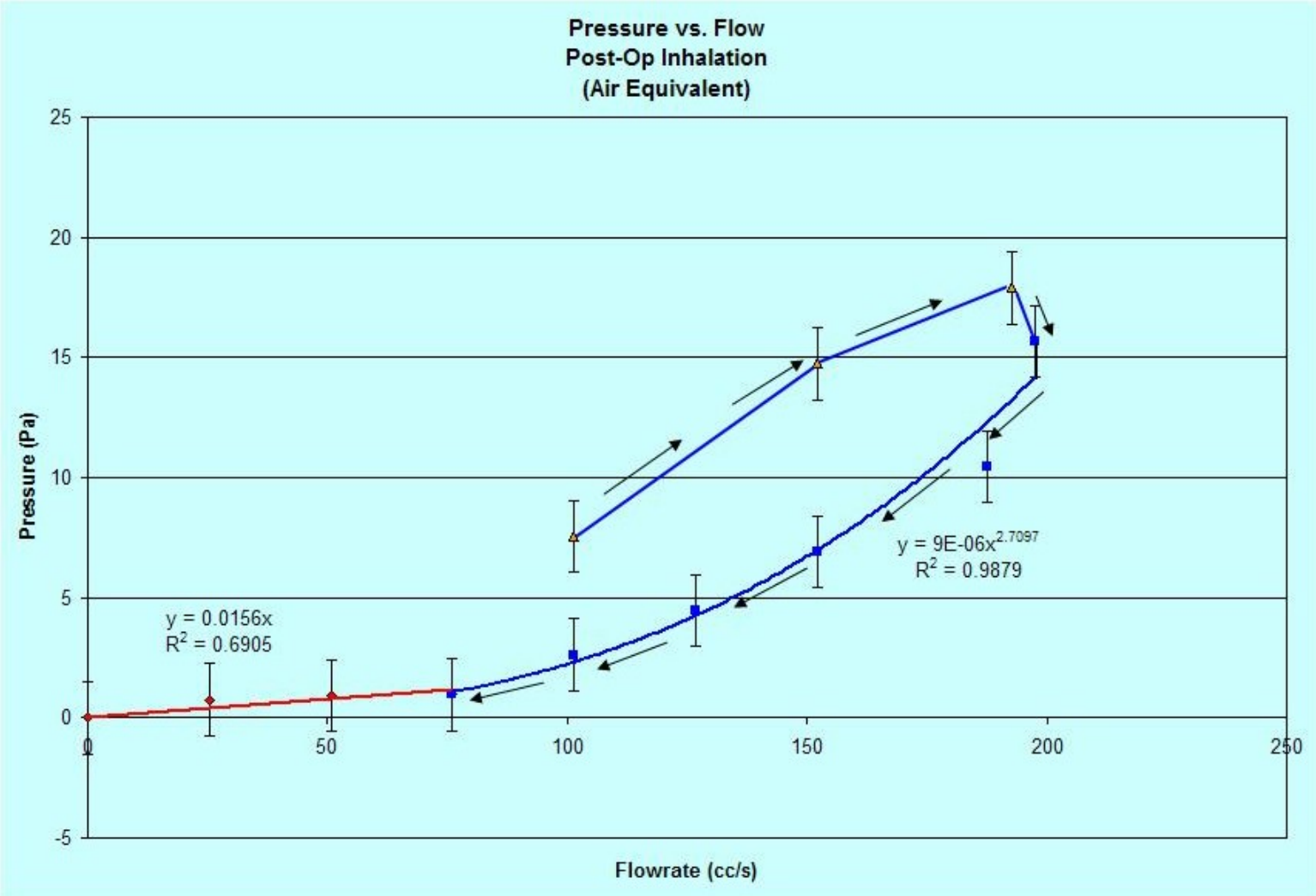

Figure 6.2 Inhalation: pressure versus flow, post-nasal turbinectomy

Figure 6.3 and Figure 6.4 show the results for exhalation in the pre- and post- operation nose models, respectively.

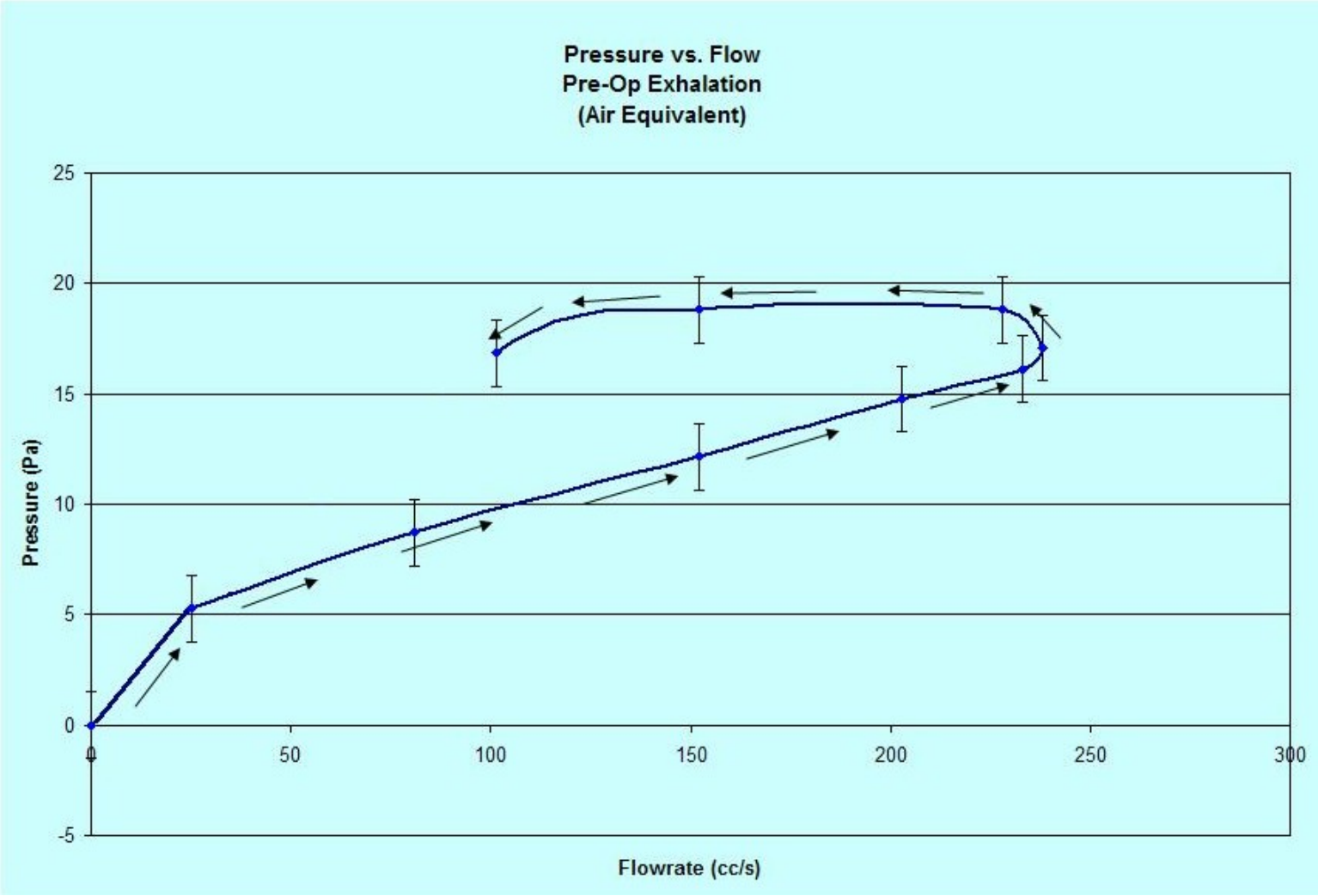

Figure 6.3 Exhalation: pressure versus flow, pre-nasal turbinectomy

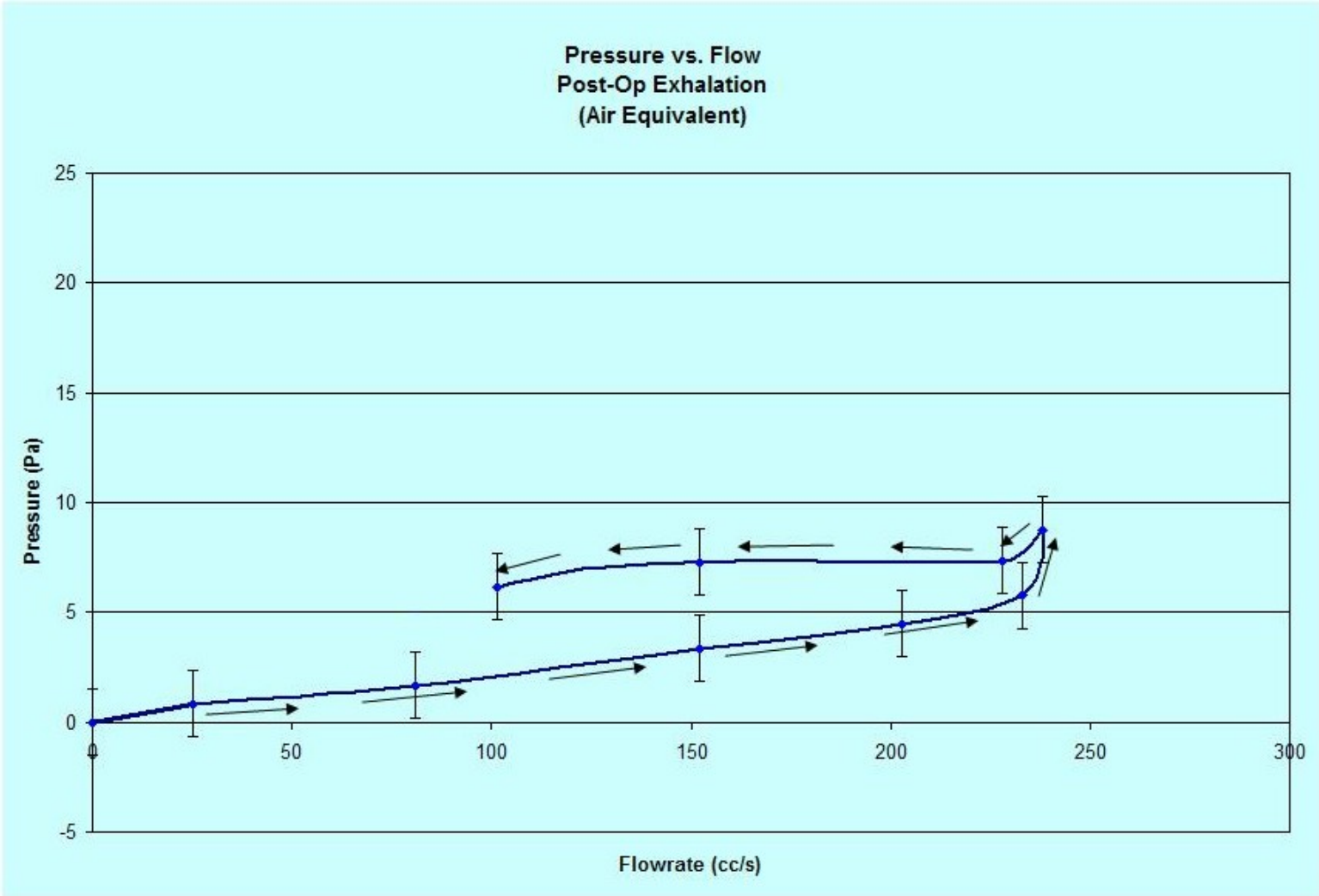

Figure 6.4 Exhalation: pressure versus flow, post-nasal turbinectomy

6.2 Statistical methods

The pressure transducer that was used was very sensitive, so there was much noise generated in the results. To smooth out the data, clarify any trends, and demonstrate stationarity of the data, a 25-term simple moving average (SMA) was used (shown in the equation below). The number of terms (n) chosen for the equation was decided upon by looking at the average number of data points collected for each cycle.

$$SMA = \frac{p_1 + p_2 + ... + p_n}{n} \qquad \textbf{Eq. 6.1}$$

An n-term SMA replaces every term in the series with the average of the n-terms before it (including that term).

Table 6.1 shows the difference between the maximum and the minimum peaks for the pre- and post-operation models.

Table 6.1 Experimental trial comparison

Summary of Data			
Model	Trial	Max Peak (Pa)	Min Peak (Pa)
Pre	1	26.2	15.1
	2	22	19.3
	3	24.1	16.0
Post	1	13.1	15.2
	2	11.0	16.5
	3	16.5	11.7

It is also necessary to point out that each individual trial had profiles that were very repeatable. Between trials the waves were only minimally different (raw data can be found in the Appendix).

To test for statistical significance, an unpaired t-test (shown in the following equation) was used, where the means of the two groups were subtracted and divided by the standard deviation.

$$t = \frac{\overline{X}_1 - \overline{X}_2}{s} \qquad \textbf{Eq. 6.2}$$

The result for the maximum pressure difference was a t-value of 1.86, with 11 degrees of freedom, and this corresponds to a p-value of $0.025 < p < 0.05$, which indicates that the pre- and the post-operation models have a clear difference in maximum

pressure difference, similarly the t-value for the minimum pressure differences was also less than 0.05 which indicates that the minimum pressure differences are also statistically different. This suggests that the surgery does affect the pressure difference within the nasal cavity during inhalation (i.e. it is easier for the patient to breathe), as well as affecting exhalation pressures. It is generally easier for patients to breathe out even before surgery and this research shows that surgery minimizes resistance when breathing out also, which is consistent with previous studies and medical literature.

6.3 Visualization imagery

The pictures below represent the visual results achieved when dye was injected into the water during a breathing cycle. During inhalation, the dye was slowly injected into the water and it was observed to break up very easily during the first 1-2 seconds of the cycle, possibly indicating turbulence.

Because the nasal models are almost clear, it can be hard for one to visualize the turbinates and the inner geometry of the nose, so pictures were taken of both the pre- and post-operation models and super-imposed lines indicating the different nasal passages and turbinates Figure 6.5.

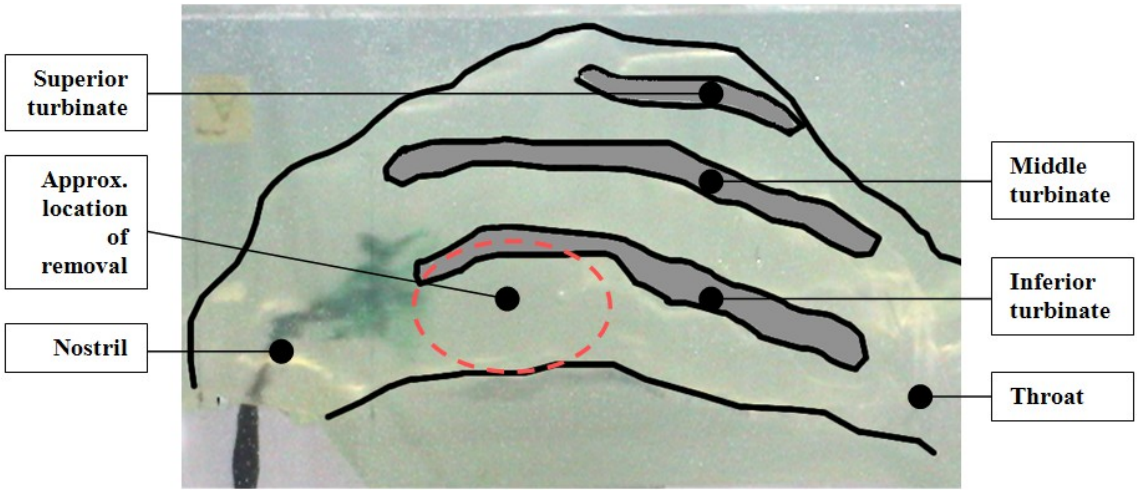

Figure 6.5 Side view of the pre-operation model, indicating turbinates, surgical location and flow direction.

The series of pictures of the pre- and post-op nasal models while the breathing cycles were set to breathe in are represented in Figure 6.6 and Figure 6.7 (full resolution pictures can be seen in the Appendix).

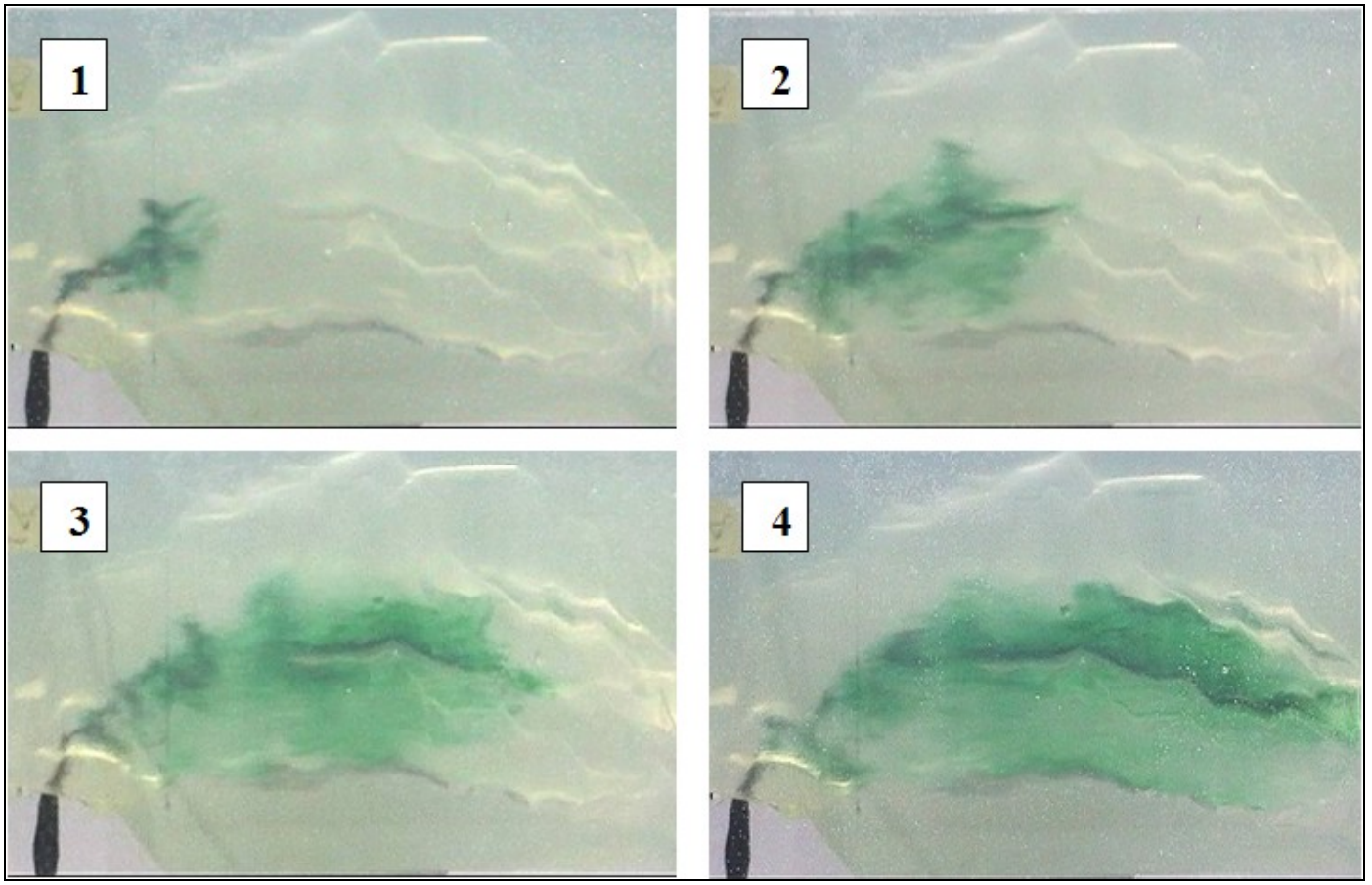

Figure 6.6 Dye visualization in the pre-op nasal model. The pictures are numbered to show progression over time of the dye in the nasal cavity.

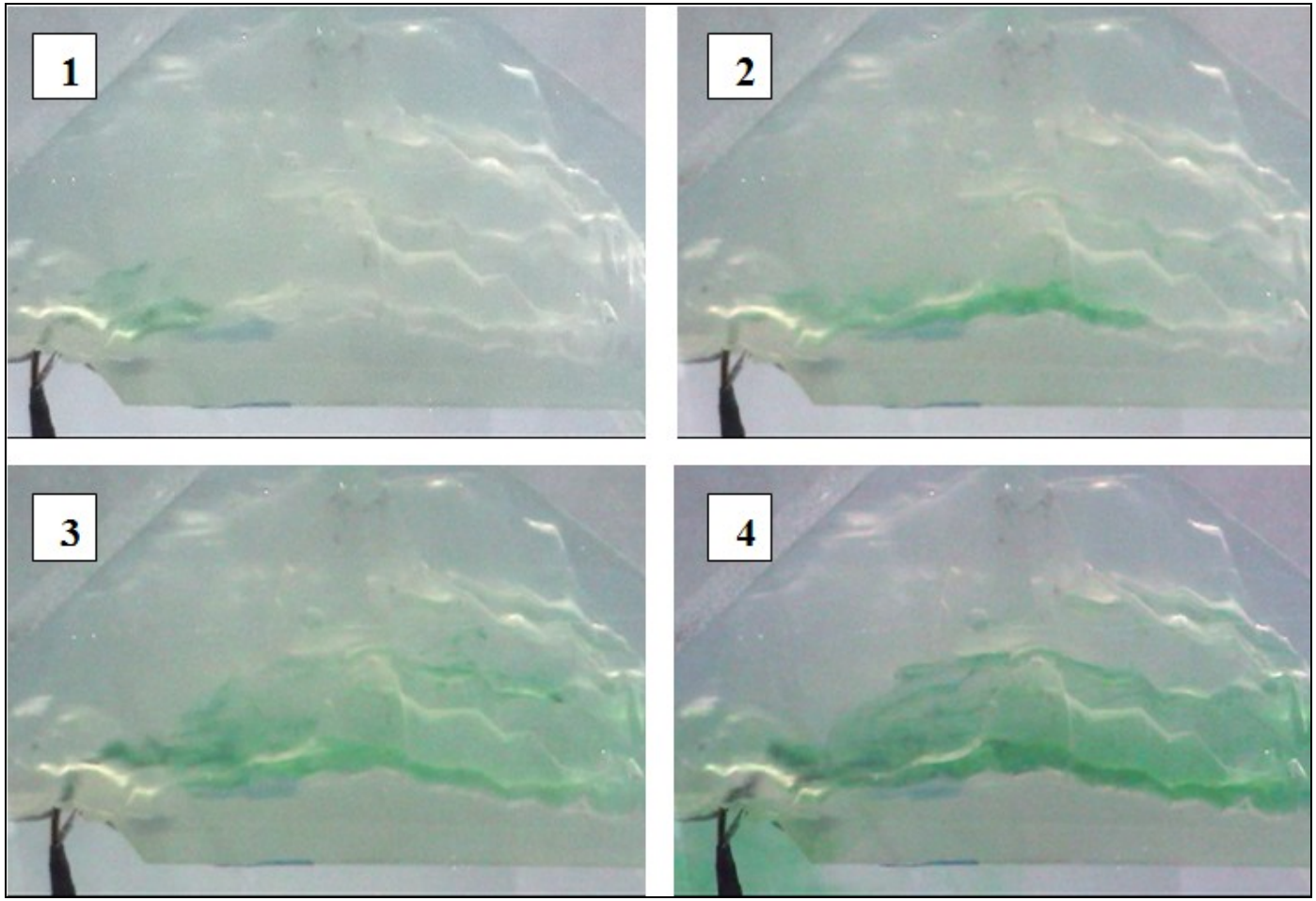

Figure 6.7 Dye visualization in the post-op nasal model

Figure 6.8, as shown below, is one still image taken from the approximately half way through the exhalation cycle. It demonstrates that the flow within the nasal cavity is laminar and there is no flow separation at all. Though this image is taken from the pre-operation model it is representative of both the pre- and post-operation exhalation cycle.

Figure 6.8 Dye visualization in pre-op nasal model during expiration.

Chapter 7: Analysis and Discussion

After several trials were conducted for the pre- and post-operation nose models an analysis of the data could be conducted. For organizational purposes the analysis will be broken down into two sections: pressure-flow analysis and visualization analysis.

7.1 Pressure and flow

When looking at the pressure versus flow rate curve as presented in Figure 6.1, it is evident that the data demonstrate linearity from flow rates of approximately 0-50cc/s. It is evident from the graph that this region is arguably laminar. The point of transition from laminar flow to that of flow separation can be predicted in the range of 50-100cc/s. Again, this is a value for one nostril; so if doubled for both nostrils this finding is consistent with the literature. The relation of nonlinearity as a result of turbulence is consistent with the data collected from a previous study (refer to Figure 2.9), which found the transitional point to be at flow rates greater than 300 cc/s [13]. Although the numerical value of transition to nonlinearity for this project does not match that of the previous study, it should be noted that non-linearity does not imply turbulence, but turbulence implies non-linearity. In addition, Figure 2.6, as generated by Weinhold and Mlynski, demonstrates similar relationships. For flow rates greater than approximately 100 (cc/s), the pressure curve increasing exponentially suggested a transition to turbulent flow.

In further support of the validity of the experimental data, an uncertainty analysis was performed on the device itself. The objective was to identify any uncertainty that resulted from external loads or vibrations. To perform this analysis the experimental set-up was run without allowing the piston to be driven. This would allow for a collection of data to explain any variations of measurements that may have occurred due solely to vibrations in the motor itself. After taking a mean and a median of the resulting data from the data acquisition equipment and considering the resolution of our data acquisition equipment, the final result of this analysis was an uncertainty of ±0.25 Pa. Though it is important to account for this uncertainty it is also evident that the uncertainly has little or no effect on the results. In addition to the uncertainty analysis done on the device, a statistical analysis was done on the pressure data. The averaged standard deviation for the

normal data was found to be 1.5 Pa. The averaged standard deviation for the post nose was 1.7Pa. The standard deviation is represented by error bars on the pressure versus flow curve.

The next important hypothesis to validate was the prediction, that there would be noticeable pressure differences in the human nasal cavities between pre- and post-operation. From Figure 6.1 and Figure 6.2 it is evident that the pressure difference differs in the nasal cavity from the pre-operation model to the post-opeartion models. A calculation of the mean percentage change of pressure drop across the cycle shows that the average decrease in pressure was approximately 45%. This data suggests that the nasal turbinectomy indeed reduces the pressure difference across the nose for both inhaling and exhaling, by opening up the airways to facilitate breathing.

An unexpected phenomenon that was observed was a hysteresis. Looking at the plots for inhalation, when the flow starts to decelerate, the pressure difference is significantly lower for any given flow rate. That same flow rate corresponds to a higher pressure at the beginning of the inhalation process. Opposite for exhaling, for a given flow rate the pressure difference is significantly higher as the flow starts to decelerate to initialize inhalation, where that same flow rate corresponded to a lower pressure at the beginning of the exhalation process. For the post-operation nose the fluctuations in pressure as a result of the hysteresis was about 6 Pa ± 3.2 Pa for inhale and 4 Pa ± 3.2 Pa for exhale. For the pre-operation nose the difference in pressure was 3 Pa ± 3 Pa for inhalation and 6 Pa ± 3 Pa for exhalation. The fact that each set of values is accompanied by different uncertainties is a result of the post data having a standard deviation of 1.7 Pa and the normal having a standard deviation of 1.7 Pa.

7.2 Visualization

The visuals captured from the models depict a clear difference in flow. The pre-op model had much of dye directed towards the middle part of the nose, whereas the post-op model had dye mostly at the bottom. Although it was not possible to look at the imaging frame by frame, it was speculated that a vortex developed in the pre-operation model. Further insight was extracted that the vortex blocked flow to the inferior turbinate.

Thus, it was concluded that the turbinectomy altered the flow separation, which allowed more flow to be directed to the inferior turbinate.

In this experiment the flow was characterized as predominantly laminar throughout most of a breathing cycle. In the pre-operation nose model flow appeared to break up quickly when entering the region which was later operated on after the partial nasal turbinectomy. It was also noted that the majority of the dye that was injected into the flow path was directed into the inferior and middle turbinates. Very little flow was directed into the superior turbinate. This concurs with the previous nasal flow studies of the nasal physiology [13]. In observing the flow in the post-operation nose the flow did not break up as it did in the pre-operation nose. The flow was considerably laminar as it was directly mostly towards the inferior turbinate. There was noticeable difference in the flow as the dye approached the area which was removed from the inferior turbinate. It was determined that there was mainly flow separation and very little turbulent mixing.

7.3 Summary of findings

The turbinectomy tended to have several effects on the pressure versus flow relation. In the post-operation nose model, the point at which there was an onset of flow separation shifted from 50cc/s to 75cc/s. Second the pressure differential tended to be reduced for a given flow rate in the post-operation nose model. This held true for both inhalation and exhalation. Last the differential that arose as a result of the hysteresis was increased for inhalation and decreased for the exhalation.

The fact that there was an increased value of flow that identified the onset of nonlinearity as a result of the turbinectomy gave speculation as to whether the flow was laminar or turbulent. It is evident that the turbinectomy increased the opening within the nasal passage, thus the only fair conclusion was that the Reynolds number was lowered for given flow rates. Looking at the Reynolds number, when the diameter is increased, the Reynolds number is decreased by that factor: thus, to compensate for that decrease in Reynolds, it is necessary to have an increase in flow rate. It is clear that there was flow separation identified by the nonlinearity, but the fact that the onset of nonlinearity was governed by the Reynolds number justifies the speculation that the flow separation was characterized by turbulence.

Comparing the pressure versus flow curves for the pre and post model, it is evident that surgery lowered the total resistance to flow. On average the percentage difference was roughly 45%.

$$P_1 - (P_2 + \frac{1}{2}\rho V_2^2) - \rho g(z_2 - z_1) = h + \frac{1}{2}\rho V_1^2 + \rho \int_1^2 \frac{dQ/A}{dt} ds \qquad \textbf{Eq. 7.1}$$

Looking at the following expression it is evident that a turbinectomy will reduce the magnitude of the acceleration term resulting in a lower pressure differential. But the acceleration term has no bearing on the maximum peak since at maximum pressure you have no change in velocity. Therefore since it is evident that the velocity squared at the inlets and outlets is unaltered, the changes must have occurred in the head loss.

During the experiment it was evident that there was hysteresis in the pressure versus flow curve. During the inhalation after the peak pressure had been reached in the cycle it was evident that this phenomenon lowered that pressure value for a given flow rate. Referring to previous equation, this phenomenon can be attributed solely to the unsteady acceleration term. Prior to when the maximum pressure peak is reached the acceleration is positive, but ounce the maximum pressure has been obtained the acceleration term is negative thus reducing the pressure differential. To provide further evidence it was found that the magnitude of this term was of the order of 3-5Pa, which is roughly what was observed as a result of the hysteresis. The calculation is shown below.

$$\rho \int_1^2 \frac{dV}{dt} ds \cong \rho \left(\frac{dV}{dt} \right)_{avg} S \qquad \textbf{Eq. 7.2}$$

S was found to range from 200mm to 300mm. This is a result of the multiple channels that make up the nasal passages. The maximum acceleration was found to be 17 mm/s^2, thus

$$1000 \frac{kg}{m^3} \times .017 \frac{m}{s^2} \times .25m = 4.25Pa \qquad \textbf{Eq. 7.3}$$

Scaled to air estimates the term to have a magnitude of

$$\Delta P = \Delta P^* \frac{\rho}{\rho^*} \left(\frac{Q}{Q^*} \frac{A^*}{A} \right)^2$$

$$\Delta P = \Delta P^* 1.08 \qquad \textbf{Eq. 7.4}$$

$$4.59PA = 4.25Pa \times 1.08$$

Chapter 8: Conclusions

After completing this experiment, several key conclusions were made as a result of the findings. The conclusions presented below only provide a brief insight into the understanding of unsteady-state flow characteristics of the human nasal cavity, but still offer ample evidence that suggests that further studies of flow through the human nasal cavity cannot be modeled as quasi-steady-state.

- Between pre- and post-operation models there was a reduced pressure drop
- Between pre- and post-operation models there was an increase in the flow-rate that identified a non-linear pressure-flow relationship.
- For both inhalation and exhalation a hysteresis was identified

In the post operation nose model, the point at which there was an onset of flow separation shifted from 50 cc/s to 75 cc/s. This increased flow rate, which identified the onset of nonlinearity and was a result of the turbinectomy, gives reasonable evidence that the surgery resulted in a shift in the critical Reynolds number; a higher critical Reynolds number implies that increased flow rates will still result in a linear-laminar flow region.

When comparing the pressure versus flow curves for the pre- and post-operation models, it is evident that the surgery influenced the total flow resistance across the nose during breathing because a decreased pressure drop was measured. It was found that during inhalation the maximum pressure drop was approximately 27.2% lower in the post-operation nose model than it was in the pre-operation nose model. For the exhalation the maximum pressure drop was lowered by 48.7%. This data verifies that the surgical procedure does indeed reduce the amount of resistance during breathing within the nasal cavity.

A hysteresis was observed in the pressure versus flow curve during normal breathing; this can only be seen in unsteady flow. During inhalation and after the peak pressure had been reached in the cycle (decelerating flow), it was evident that this phenomenon lowered the pressure values for a given flow rate. In contrast, this phenomenon raised the pressure values for a given flow rate. As a result of the observation of the hysteresis, it can be concluded that flow inside the nasal cavity can not be modeled as quasi-steady.

Chapter 9: Recommendations

Based on the previous experience many modifications could be applied to assure future improvements. Studies should ensure a more realistic simulation of normal, adult breathing. This is justified because scaling the numbers to simulate an adult breathing cycle (with the double-sized nasal models) using water would involve about 3-5 liters of water, and the frictional forces would be easier to overcome if a future project team used many small pistons instead of just one large.

With regards to testing and visualization, it is suggested that future research try to put the pressure transducer or dye injector at different locations in the nostril. This will allow one to see if different results can be obtained. The visuals produced were very helpful and crucial to proving the findings. The Omega pressure transducer was very sensitive; as a result, putting the transducer tubes at different locations might produce different readings. In terms of the pressure transducer setup, what is important to note is that in the inhalation and exhalation the pressure differential that was measured was not due solely to the head loss, but also due to the dynamic pressure and the unsteady acceleration, where adding or subtracting varies for inhalation and exhalation. What would be beneficial for future studies is to figure a way so as to always be measuring the total pressure.

$$P_1 + \rho\frac{1}{2}V_1^2 + \rho g z_1 = P_2 + \rho\frac{1}{2}V_2^2 + \rho g z_2 + h + \rho\int_1^2 \frac{dV}{dt}ds \qquad \textbf{Eq. 9.1}$$

Thus,

$$P_{1total} - P_{2total} = h + \rho\int_1^2 \frac{dV}{dt}ds + \rho g(z_2 - z_1) \qquad \textbf{Eq. 9.2}$$

In addition the study showed that regardless of the medium or any other factors the same tidal volume would be needed. It would have been difficult to construct a system that would have been capable of displacing 4.8 L of water, but it is necessary in order scale correctly.

Also, the vibrations from the spring and the motor added a large amount of noise to the pressure transducer measurements, on account of the sensitivity of the instrument. It is recommended that future research should dampen and filter out this noise, which can

be done in various ways: dampen the noise mechanically by stabilizing the device, analyzing the external loads (identify their frequency), or using a Fast Fourier Transform (FFT) to map the signal to a frequency domain instead of a time domain are all options.

References

[1] "Turbinectomy Definition." (MedicineNet, Inc: 2006). <http://www.medterms.com/script/main/art.asp?articlekey=11217>.

[2] Lane, A.P. "Nasal anatomy and physiology." *Facial Plastic Surgery Clinics of North America*, Vol. 12 (2004): 387-95.

[3] Hörschler, I., Ch. Brücker, W. Schröder, M. Meinke. "Investigation of the impact of the geometry on the nose flow." *European Journal of Mechanics B/Fluids*, Vol. 25 (2006): 471–90.

[4] Cook, P.R., Begegni, A., Bryant, W.C., and Davis, W.E. "Effect of partial middle turbinectomy on nasal airflow and resistance." *Otolaryngology – Head and Neck Surgery*, Vol. 113 (1995): 413-19.

[5] Kane, Kevin J. "Persistent sinusitis from recirculating mucus after inferior turbinectomy." *International Congress Series* 1240 (2003): 463-67.

[6] Fenn, W.O., and Rahn, H. Handbook of Physiology: Respiration. Washington: American Physiological Society, 1964.

[7] Hahn, I., Scherer, P. W., and Mozell, M. M. "Velocity profiles measured for airflow through a large-scale model of the human nasal cavity." *Journal of Applied Physiology*, Vol. 75 (1993): 2273-87.

[8] Keyhani K., Scherer, P. W., and Mozell, M. M. "Numerical simulation of airflow in the human nasal cavity." *Journal of Biomedical Engineering*, Vol. 117 (1995): 429-41.

[9] Kelly, J.T., Prasad, A.K., and Wexler, A.S. "Detailed flow patterns in the nasal cavity." *Journal of Applied Physiology*, Vol. 89 (2000): 323-37.

[10] Weinhold, I., Mlynski, G. "Numerical simulation of airflow in the human nose." *Eur Arch Otorhinolaryngol*, Vol. 261 (2004): 452-55.

[11] Bailie, N.A. "Numerical Modeling of Nasal Airflow." *Otolaryngology – Head and Neck Surgery*, Vol. 131 (2004): 187-88.

[12] Chruchill, S.E., Shackelford, L.L., Georgi, S.J., and Black, M.T. "Morphological Variation and Airflow Dynamics." *American Journal of Human Biology*, Vol. 16 (2004): 625-38.

[13] Learned, A., Miczek, S., and Salib, M. "Alterations in Flow Patterns through Nasal Passages due to a Turbinectomy." MQP. Worcester Polytechnic Institute, 2005.

[14] Straatman, A., Khayat, R., Haj-Qasem, E., and Steinman, D. “On the hydrodynamic stability of pulsatile flow in a plane channel.” *Physics of Fluids*, Vol. 14 (2002): 1938-1944.

Appendix A: DVD

{not included w/EPROJECT SUBMISSION}